Neoplasia • Vol. 2, Nos. 1–2, January-April 2000, pp. 89–117 89
www.nature.com/neo

Fluorescence Spectroscopy of Neoplastic and Non-Neoplastic Tissues

Nirmala Ramanujam

Department of Biochemistry and Biophysics, University of Pennsylvania, Philadelphia, PA

Abstract

Fast and non-invasive, diagnostic techniques based on fluorescence spectroscopy have the potential to link the biochemical and morphologic properties of tissues to individual patient care. One of the most widely explored applications of fluorescence spectroscopy is the detection of endoscopically invisible, early neoplastic growth in epithelial tissue sites. Currently, there are no effective diagnostic techniques for these early tissue transformations. If fluorescence spectroscopy can be applied successfully as a diagnostic technique in this clinical context, it may increase the potential for curative treatment, and thus, reduce complications and health care costs. Steady-state, fluorescence measurements from small tissue regions as well as relatively large tissue fields have been performed. To a much lesser extent, time-resolved, fluorescence measurements have also been explored for tissue characterization. Furthermore, sources of both intrinsic (endogenous fluorophores) and extrinsic fluorescence (exogenous fluorophores) have been considered. The goal of the current report is to provide a comprehensive review on steady-state and time-resolved, fluorescence measurements of neoplastic and non-neoplastic, biologic systems of varying degrees of complexity. First, the principles and methodology of fluorescence spectroscopy are discussed. Next, the endogenous fluorescence properties of cells, frozen tissue sections and excised and intact bulk tissues are presented; fluorescence measurements from both animal and human tissue models are discussed. This is concluded with future perspectives. *Neoplasia* (2000) **2,** 89–117.

Keywords: fluorescence spectroscopy, cell, tissue, *in vivo*, neoplasia.

Introduction

Diagnostic techniques based on fluorescence spectroscopy have the potential to link the biochemical and morphologic properties of tissues to individual patient care. In particular, these techniques are fast, non-invasive and quantitative. Furthermore, they can be used to elucidate key tissue features, such as the cellular metabolic rate, vascularity, intra-vascular oxygenation and alterations in tissue morphology. These tissue features can be interpreted to shed light on a variety of clinical problems, such as neoplasia and atherosclerosis. If applied successfully, fluorescence spectroscopy has the potential to represent an important step forward toward advances in diagnostic and therapeutic medical applications.

One of the most widely explored applications of fluorescence spectroscopy is the detection of endoscopically invisible, early neoplastic growth in epithelial tissue sites. Early neoplastic growth refers to pre-malignant changes such as dysplasia and carcinoma *in situ* (CIS), which precede malignancy, i.e., invasive carcinoma. Currently, there are no effective diagnostic techniques for these early tissue transformations. Fluorescence spectroscopy is ideally suited for this application because of its ability to examine tissue surfaces, rather than tissue volumes, and its adaptability to an endoscopic device. If fluorescence spectroscopy can be applied successfully as a diagnostic technique in this clinical context, it may increase the potential for curative treatment, and thus, reduce complications. In addition to the potential for improved patient outcome, the fast and non-invasive nature of this diagnostic technique may also reduce health care costs.

Steady-state, fluorescence measurements from small tissue regions (less than a few millimeters in diameter) as well as relatively large tissue fields (a few centimeters in diameter) have been performed [1,2]. To a much lesser extent, time-resolved, fluorescence measurements are also being explored, currently [1,2]. Furthermore, sources of both intrinsic (endogenous fluorophores) and extrinsic fluorescence (exogenous fluorophores) have been considered [1,2]. The advantage of using exogenous fluorophores is that the photophysical and pharmocokinetic properties can be selected and are known. Furthermore, exogenous fluorophores are more highly fluorescent than endogenous fluorophores. However, the disadvantage of using exogenous fluorophores is that issues relating to safety and toxicity of the drug being used have to be addressed. Furthermore, the selection of the optimal time delay after administration of the drug is non-trivial.

Abbreviations: ROC, receiver-operator curve; SIL, squamous intraepithelial lesion; SCC, squamous cell carcinoma; CIS, carcinoma *in situ*; DMBA, dimethylbenz[*a*]anthracene; NMBA, *N*-nitrosomethyl benzylamine; 4NQO, 4-nitroquinoline 1-oxide.

Address all correspondence to: Dr. Nirmala Ramanujam, Department of Biochemistry and Biophysics, University of Pennsylvania, D501 Richards Building, Philadelphia, PA 19104.
E-mail: nimmi@mail.med.upenn.edu

Received 12 November 1999; Accepted 2 December 1999.

Several authors have reviewed the progress in this field over the last decade. Andersson-Engels *et al.* [3,4] discussed the possibilities of using fluorescence spectroscopy for tissue diagnosis. The tissue types discussed were malignant tumors and atherosclerotic lesions. Studies of endogenous fluorescence as well as exogenous fluorescence with contrast agents were also presented. In a subsequent review, Andersson-Engels and Wilson [5] reviewed the scientific, technical and practical issues related to the use of fluorescence spectroscopy for tissue diagnosis in clinical oncological applications. Papazoglou [6] presented a review on the diagnosis of malignancies and atherosclerotic plaques using fluorescence spectroscopy. Special emphasis was given to problems, which were raised during clinical trials and recent experimental studies, such as the identification of the fluorescent chemical species and the determination of the illumination/collection geometry for fluorescence spectroscopy. Bigio and Mourant [7] reviewed fluorescence spectroscopy and elastic scattering spectroscopy of small regions of tissue, whereas Andersson-Engels *et al.* [8] focused on fluorescence spectroscopy of relatively, large tissue fields. More comprehensive reviews have been written by Richards-Kortum and Sevick-Muraca [2] and Wagnieres *et al.* [1]. The former review focuses on the quantitative aspects of fluorescence spectroscopy. Specifically, this review describes optical interactions pursued for biomedical applications, provides a descriptive framework for light interactions in tissue and finally, reviews the important endogenous and exogenous molecules and how they are exploited for tissue diagnosis. The latter review, which focuses more on clinical aspects, presents a critical status report on the diagnosis of neoplastic tissues, *in vivo* using fluorescence spectroscopy.

The goal of the current report is to provide a comprehensive review on steady-state and time-resolved, fluorescence measurements of neoplastic and non-neoplastic biologic systems of varying degrees of complexity. First, the principles and methodology of fluorescence spectroscopy are discussed. Next the endogenous fluorescence properties of cells, frozen tissue sections and excised and intact bulk tissues are presented; fluorescence measurements from both animal and human tissue models are discussed. It should be noted that the emphasis of this review is on fluorescence spectroscopy of endogenous tissue fluorescence. The reader is directed to the review article of Wagnieres *et al.* [1] for a detailed review on fluorescence spectroscopy of exogenous tissue fluorophores. Finally, this report concludes with a brief discussion of future applications, novel technologies and quantitative modeling techniques for elucidating the biochemical/morphologic basis of fluorescence spectroscopy.

Principles and Methodology of Fluorescence Spectroscopy

When a biologic molecule is illuminated at an excitation wavelength, which lies within the absorption spectrum of that molecule, it will absorb this energy and be activated from its ground state (state of lowest energy; S_0) to an excited state (state of higher energy; S_1). The molecule can then relax back from the excited state to the ground state by generating energy in the form of fluorescence, at emission wavelengths, which are longer than that of the excitation wavelength. This is illustrated schematically in Figure 1.

The phenomenon of fluorescence displays several general characteristics for a particular biologic molecule [9]. First, due to losses in energy between absorption and emission, fluorescence occurs at emission wavelengths, which are always red-shifted, relative to the excitation wavelength. Second, the emission wavelengths of fluorescence are independent of the excitation wavelength. Third, the fluorescence spectrum of a biologic molecule is generally a mirror image of its absorption spectrum.

The fluorescence of a biologic molecule is characterized by its quantum yield and its lifetime [9]. The quantum yield is simply the ratio of the number of photons emitted to the number absorbed. The lifetime is defined as the average time the biologic molecule spends in the excited state before return to the ground state. The fluorescence quantum yield and lifetime are modified by a number of factors that can increase or decrease the energy losses. For example, a molecule may be non-fluorescent as a result of a large rate of non-radiative decay (thermal generation) or a slow rate of radiative decay (fluorescence).

Fluorescence spectroscopy is the measurement and analysis of various features that are related to the fluorescence quantum yield and/or lifetime of a biologic molecule(s). The fluorescence intensity of a biologic molecule is a function of its concentration, its extinction coefficient (absorbing power) at the excitation wavelength, and its quantum yield at the emission wavelength [10]. A fluorescence emission spectrum represents the fluorescence intensity measured over a range of emission wavelengths, at a fixed excitation wavelength. Conversely, a fluorescence excitation spectrum is a plot of the fluorescence intensity at a particular emission wavelength, for a range of excitation wavelengths. A fluorescence, excitation-emission matrix (EEM) is a two dimensional contour plot, which displays the fluorescence intensities as a function of a range of excitation and emission wavelengths. Each contour represents points of equal fluorescence intensity. Finally, fluorescence lifetime measurements are represented as the fluorescence intensity distributed over a very short time scale, at a fixed excitation-emission wavelength pair. (Figure 2, $a-d$) shows an

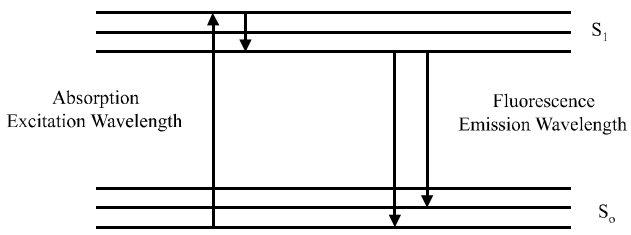

Figure 1. *Energy level diagram illustrating the phenomena of absorption and fluorescence.*

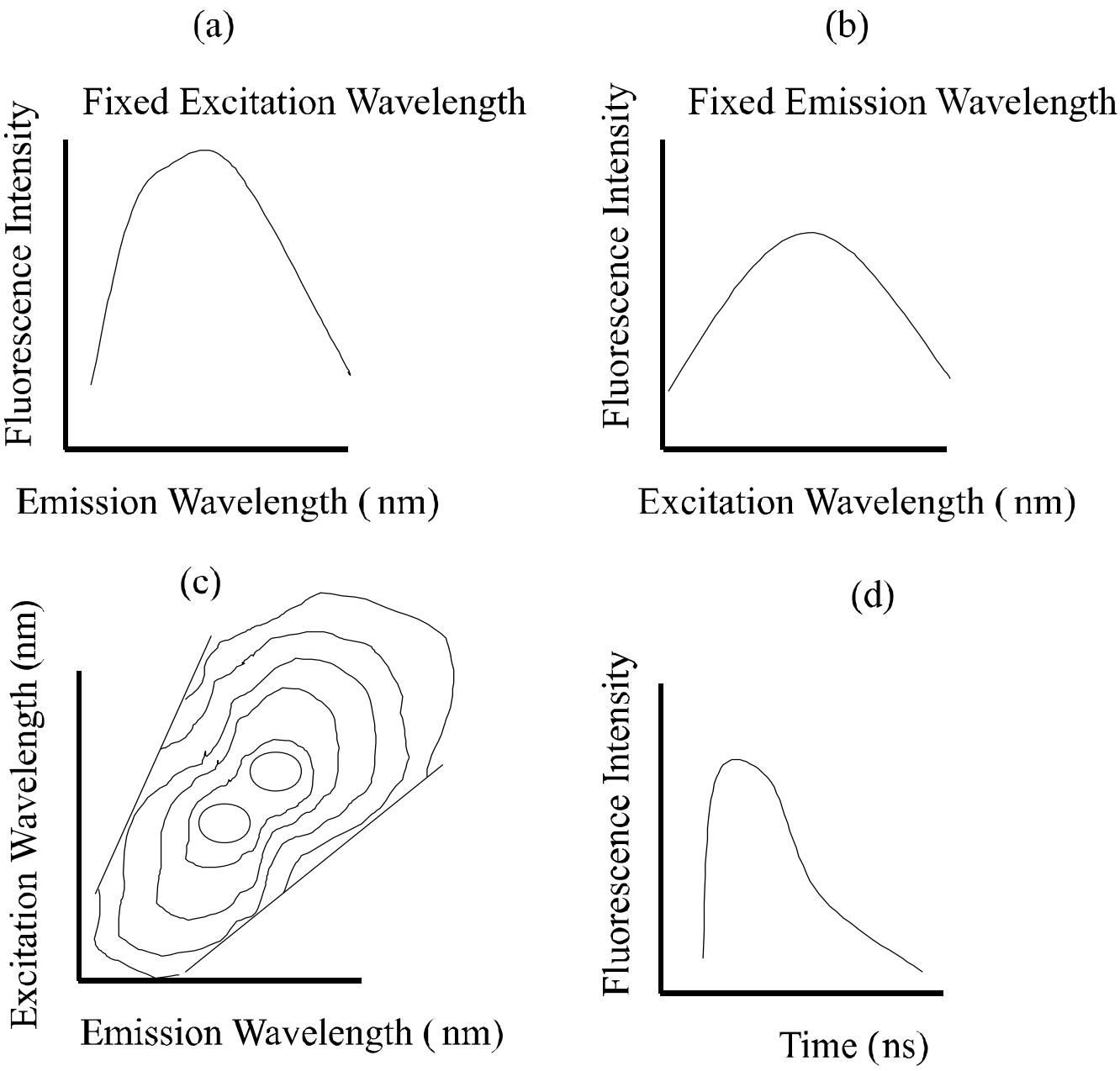

Figure 2. *Illustration of a fluorescence (a) emission spectrum, (b) excitation spectrum, (c) excitation-emission matrix (EEM) and (d) decay profile.*

illustration of a fluorescence (a) emission spectrum, (b) excitation spectrum, (c) EEM and (d) decay profile.

Table 1 shows a list of biologic molecules, which exhibit endogenous fluorescence and their excitation and emission maxima [2,11,12]. These endogenous fluorophores include the amino acids, structural proteins, enzymes and co-enzymes, vitamins, lipids and porphyrins. Their excitation maxima range lies between 250 and 450 nm (spans the ultraviolet and visible spectral range), whereas their emission maxima range lies between 280 and 700 nm (spans the ultraviolet, visible and near-infrared spectral range). Details of the molar extinction coefficients, fluorescence quantum yields and lifetimes are provided elsewhere [2]. Fluorophores that are speculated to play a role in transformations that occur in the neoplastic process, are the amino acids, tryptophan and tyrosine [13,14], structural proteins, collagen and elastin [15–21], the co-enzymes, NADH [13,22] and FAD [22,23] and porphyrins [24].

Fluorescence spectroscopy of turbid media such as tissue depends on one or more of the following. Specifically, it depends on the concentration and distribution of fluorophore(s) present in the tissue, as well as the biochemical/biophysical environment, which may alter the quantum yield and lifetime of the fluorophore(s). For example, epithelial tissues, generally have two primary sub-layers: a surface epithelium and an underlying stroma or submucosa; the specific fluorophores, as well as their concentration and distribution can vary significantly between these two tissue

Table 1. Excitation and Emission Maxima of Endogenous Fluorophores.

Endogenous fluorophores	Excitation maxima (nm)	Emission maxima (nm)
Amino acids		
Tryptophan	280	350
Tyrosine	275	300
Phenylalanine	260	280
Structural proteins		
Collagen	325, 360	400, 405
Elastin	290, 325	340, 400
Enzymes and coenzymes		
FAD, Flavins	450	535
NADH	290, 351	440, 460
NADPH	336	464
Vitamins		
Vitamin A	327	510
Vitamin K	335	480
Vitamin D	390	480
Vitamin B_6 compounds		
Pyridoxine	332, 340	400
Pyridoxamine	335	400
Pyridoxal	330	385
Pyridoxic acid	315	425
Pyridoxal 5′-phosphate	330	400
Vitamin B_{12}	275	305
Lipids		
Phospholipids	436	540, 560
Lipofuscin	340 – 395	540, 430 – 460
Ceroid	340 – 395	430 – 460, 540
Porphyrins	400 – 450	630, 690

NADH, reduced nicotinamide dinucelotide; *NAD(P)H*, reduced nicotinamide dinucleotide phosphate; *FAD*, flavin adenine dinucleotide.

layers. Fluorescence spectroscopy of turbid media such as tissue also depends on the absorption and scattering that results from the concentration and distribution of non-fluorescent absorbers and scatterers, respectively, within the different sub-layers of the tissue.

The effect of the aforementioned variables on fluorescence spectroscopy of tissue is wavelength-dependent. First, the fluorophores that have absorption bands that lie in the same wavelength range as the excitation light will be excited and hence, emit fluorescence. The absorption and scattering properties of the tissue will affect light at both these excitation and emission wavelengths. Therefore, only those fluorophores contained in the tissue layers to which the excitation light penetrates and from which, the emitted light can escape the tissue surface will produce measurable fluorescence. Elastic scattering events in tissue are caused by random spatial variations in the density, refractive index, and dielectric constants of extracellular, cellular and subcellular components [25]. Tissue scattering generally decreases monotonically with increasing wavelength over the ultraviolet, visible and near-infrared spectral regions [2]. Absorption in tissue over the same spectral range is primarily attributed to hemoglobin [26]. Although absorption in tissue is strongly wavelength-dependent, it tends to generally decrease with increasing wavelengths [2]. Consequently, the penetration depth of light, which is primarily a function of the tissue absorption properties, decreases from several centimeters to a few hundred microns, from the near-infrared to the ultraviolet [2]. For example, in the UV spectral region, the penetration depth of light in tissue is approximately 225 μm at 337 nm [27].

The illumination and collection geometry of the excitation and the emitted light, respectively, can also affect the fluorescence measurement from tissue, with respect to both the intensity and line shape [28]. This may be attributed to the fact that although the fluorescence is generated isotropically from the fluorophores within a medium, the fluorescence emitted from its surface may range from isotropic to anisotropic depending on whether the medium is highly absorbing, dilute or turbid [29]. Monte Carlo simulations have been used extensively to simulate light distribution in turbid media to explore the effect of absorption and scattering on the fluorescence emitted from the surface, using finite excitation beam profiles and complex excitation and emission geometries [29,30]. The most useful excitation and emission geometry is one that yields fluorescence measurements that are independent of geometric dependencies. As shown elsewhere [28], design of an optical fiber probe configuration that consists of a geometry in which the emitted light from the tissue is collected only from that surface directly illuminated by the excitation light, fulfills this criterion.

Steady-state and to a lesser extent, time-resolved, fluorescence measurements have been performed on biologic fluids, single cells, cell suspensions, frozen tissue sections and from bulk tissues, both *in vitro* and *in vivo*. The various types of instruments employed for these measurements, essentially have the same basic components, except for a few differences. A schematic of the basic components of such an instrument is shown in Figure 3. It consists of a monochromatic excitation light source, a flexible, delivery and collection conduit for the delivery of excitation light to and the collection of the emitted light from

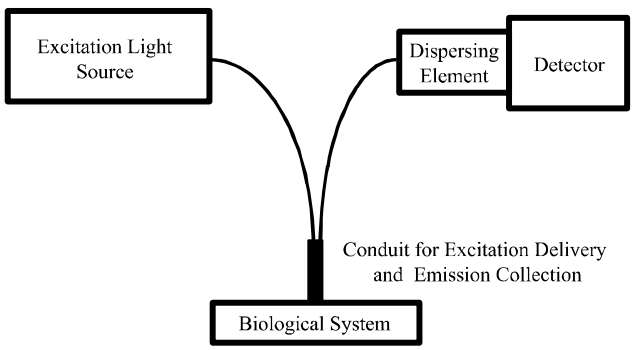

Figure 3. *Schematic of the basic components of an instrument employed for fluorescence spectroscopy of biological media.*

the biologic medium, a dispersing element, which separates the emitted light into its respective wavelengths and a detector, which measures the intensity at the emission wavelength(s).

Generally, monochromatic excitation light sources include ultraviolet and visible arc lamps (mercury, xenon) and continuous wave (Argon ion-ultraviolet lines, Helium-Cadmium — 442 nm) or pulsed lasers (nitrogen — 337 nm; the addition of dyes in an attached resonant cavity provides additional visible wavelengths). Lasers have the advantage of high-efficiency coupling into fiber-optic probes. However, filtered arc lamps have the advantage of excitation wavelength tunability, when used with a series of band pass filters or a monochromator (see below) and they are generally, more portable. It should be noted that pulsed lasers, with very short pulse durations (in the order of nanoseconds) are necessary when the biologic medium needs to be illuminated with pulsed excitation light for gated detection (which provides effective rejection of ambient light during florescence measurements) and for fluorescence, lifetime measurements.

With respect to illumination of and collection of light from the biologic system, two different approaches may be considered. The first approach is to use fiber-optic probes that are placed directly in contact (contact approach) and the second approach is to use a series of lenses to project the light onto the surface and collect it, in a similar manner (non-contact approach). With the contact approach, variable pressure on the biologic medium may distort the fluorescence spectrum. However, with the non-contact approach, the fluorescence intensity will vary with the variable, source-sample and sample-detector distance. In general, the contact approach is used for steady-state and time-resolved, fluorescence measurements from small tissue areas, whereas the non-contact approach is more suited for fluorescence imaging from relatively larger areas of tissue.

Light can be spectrally dispersed using a monochromator or a spectrograph, which are both dispersing components. A monochromator presents one wavelength or band pass at a time of the input light from its exit slit, whereas a spectrograph presents a range of wavelengths of the input light, simultaneously at the exit focal plane. Monochromators can be used as filters in conjunction with arc lamps to produce monochromatic excitation light at a series of wavelengths (if only several excitation wavelengths are needed, band pass filters are more appropriate). Monochromators can also be used to disperse the emitted light into its respective wavelengths, each of which can be detected serially using a single-channel detector. However, spectrographs can be used to disperse the emitted light into its respective wavelengths, simultaneously, for multi-channel detection.

The important considerations in choosing a detector are the type of measurements being made, i.e., single wavelength versus multi-wavelength and single-pixel (small area measurements) versus multi-pixel (large area measurements). Fluorescence measurements from single-pixels can be made either using a single-channel or multi-channel detector. If fluorescence intensity at only one or several wavelengths is being measured, single-channel, photo emissive tubes called photo multiplier tubes (PMT) or semi-conductor based, avalanche photodiodes (APD), with band pass filters can be used. For fluorescence spectroscopy, a spectrograph coupled to a multi-channel, photo diode array is appropriate. Fluorescence spectroscopy can also be performed using a monochromator coupled to a PMT, albeit this substantially increases the measurement time. In the case of fluorescence imaging from multiple pixels, a two-dimensional, charged coupled device (CCD) camera, with band pass filters may be employed. To reduce or eliminate the detection of ambient light, a detector with an intensifier for fast gating (several nanoseconds) must be used in conjunction with a pulsed excitation light source. Also, to minimize the detection of the back-scattered excitation light, which is much stronger than the weaker emitted light, optical components, such as long pass or dichroic filters have to be employed in front of the detection system.

A widely employed instrument for the measurement of fluorescence EEMs of biologic fluids, cell suspensions and tissues specimens (in a sample chamber), is a conventional laboratory spectrofluorometer [9]. A typical spectrofluorometer consists of a Xenon arc lamp and excitation monochromator, which serves to provide monochromatic excitation light at a range of ultraviolet and visible wavelengths, a sample chamber, and an emission monochromator and PMT, which measures the fluorescence emission spectrum, at each of these excitation wavelengths. Due to the use of an excitation and emission monochromator in this instrument, measurement times, for an entire fluorescence EEM can take as long as an hour, and clearly is impractical in a clinical setting.

Fluorescence microscopy of micro-structures in single living cells or in unstained, frozen tissue sections is typically performed using a microscope that is coupled to a lamp or laser-based excitation light source and to a series of band pass filters for fluorescence measurements at specific emission wavelengths [15–21,31]. To obtain fluorescence emission spectra of these micro-structures, the band pass filters are generally replaced by a spectrograph and a photo diode array (micro-spectrofluorometer) [19,20,23,31].

Single-pixel (<2 mm, diameter of tissue area) measurements of tissue fluorescence spectra, *in vivo* have been performed mostly using a pulsed excitation light source, a fiber-optic probe (contact approach), a spectrograph and an intensified photo diode array. The transient fluorescence decay profiles at a specific excitation-emission wavelength pair have been measured using a similar instrument, except that the spectrograph and multi-channel, photo diode array have been replaced by a filtered, single-channel PMT or APD [32]. Finally, fluorescence imaging from multiple pixels of tissue, *in vivo* (tissue area, which is a few centimeters in diameter) has been performed with a non-contact approach using a continuous wave laser in combination with a band pass filtered, CCD camera [33]. Measurements with single-

pixel and multi-pixel instruments generally require several seconds to a minute in a clinical setting.

Biologic Systems

Fluorescence Spectroscopy of Cultured Cells

Pradhan *et al.* [13] measured and compared fluorescence emission spectra and decay profiles of normal, metastatic and non-metastatic cells obtained from mice, rats and humans. The cells that were evaluated were: 1) the low metastatic and high metastatic variant of the murine melanoma cell line, 2) non-metastatic and metastatic cells from the rat rhabdomyosarcoma as well as normal skeletal muscle cells from the rat, and 3) metastatic and non-metastatic human lung squamous cell carcinoma (SCC), as well as normal human bronchiolar epithelial cells. Fluorescence emission spectra were measured in the range from 320 to 550 nm at 310 nm excitation and in the range from 400 to 600 nm at 350 nm excitation from cell suspensions in a quartz cuvette. Also, fluorescence decay profiles were measured at 340 nm, for an excitation wavelength of 310 nm, and at 440 nm, for an excitation wavelength of 350 nm from cell suspensions in a quartz cuvette. The fluorescence decay profiles were fit to single, double or triple exponential functions by the method of iterative convolution.

(Figure 4, *a* and *b*) shows the fluorescence emission spectra of metastatic and non-metastatic human lung SCC cells and normal human epithelial cells at (a) 350 and (b) 310 nm excitation. The spectra of the cells, at 340 nm excitation display a maximum at 440 nm. The spectra of the cells, at 310 nm excitation, display two maxima at 340 and 440 nm. (Figure 5, *A* and *B*) displays the fluorescence decay profile at 340 nm excitation and 440 nm emission, associated with the lamp profile (no fit curve) and that associated with the (a) non-metastatic and (b) metastatic human lung SCC cells. An evaluation of the average fluorescence lifetime of all cells evaluated at 340 nm excitation and 440 nm emission indicates that, it ranges from 0.47 to 1.9 nsec. However, the average fluorescence lifetime of all cells evaluated at 310 nm excitation and 340 nm emission, ranges from 2.4 to 3.7 nsec.

The fluorescence emission spectra and decay profiles of non-metastatic/low-metastatic and metastatic cells show that the fluorescence in the ultraviolet (340 nm) and visible (450 nm) are due to tryptophan and NADH, respectively. Evaluation of the fluorescence emission spectra indicates a distinctive increase in the fluorescence intensity for non-metastatic/low metastatic cells compared to that of metastatic cells. Furthermore, the fluorescence decay profile at 440 nm indicates that non-metastatic/low metastatic cells consistently show higher average lifetimes than metastatic and normal cells. However, at 340 nm emission, there is an increase or decrease in the average fluorescence lifetime in non-metastatic/low metastatic cells relative to their metastatic counterpart, depending on the cell type. By taking into account the fluorescence lifetime corrections to the fluorescence intensity and also the cell volume of the various cell lines, the tryptophan and NADH concentrations seem to increase consistently as the cells progress from a non-metastatic/low metastatic to metastatic state.

Anidjar *et al.* [23] characterized and compared the fluorescence emission spectra, particularly, the emission maximum, band width and intensity of urothelial normal and malignant cells in culture. The difference between this

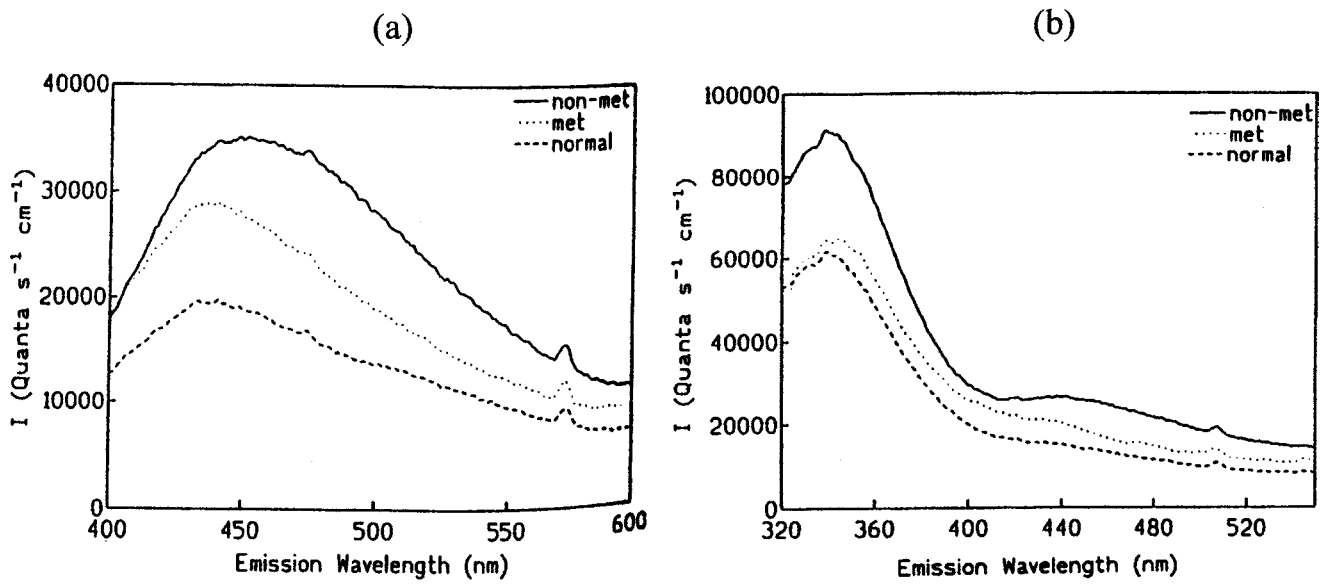

Figure 4. *Fluorescence emission spectra of metastatic and non-metastatic human lung squamous cell carcinoma (SCC) cells and normal human epithelial cells at (a) 350 nm and (b) 310 nm excitation.*

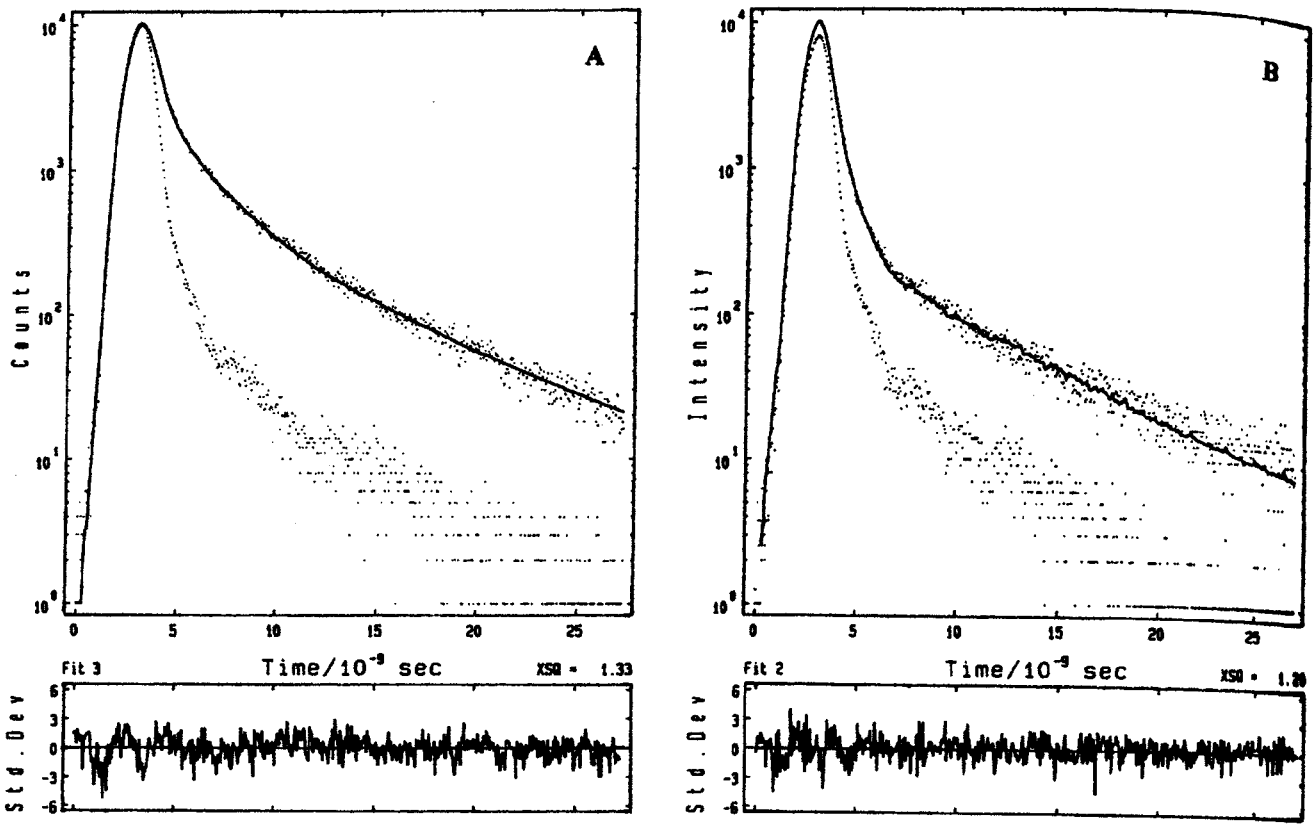

Figure 5. *Fluorescence decay profile at 440 nm associated with the lamp profile (no fit curve) and those associated with the (A) non-metastatic and (B) metastatic human lung, squamous cell carcinoma (SCC) cells.*

investigation and that done by Pradhan *et al.* [13] is that this was performed on single living cells, rather than on a suspension of living cells. Six urothelial cell types from the human bladder were used: poorly differentiated transitional cell carcinoma (TCC), poorly differentiated invasive T3 TCC, a superficial moderately differentiated TCC, a well-differentiated mature invasive epidermoid carcinoma, the human normal fetal bladder cell line and the normal urothelium. Fluorescence emission spectra were recorded from a 10-μm field within the cell at an excitation wavelength of 488 nm.

(Figure 6, *a* and *b*) displays the fluorescence emission spectra from (a) a normal urothelial cell and (b) a poorly differentiated TCC. The spectra of a subcellular volume of the normal and malignant endothelial cells are broad band with a maximum located at 550 to 560 nm. Statistical analysis of maximum emission wavelengths confirmed the lack of any significant difference between normal and malignant cells. However, the band width of the normal cells was as much as 40% larger than that observed for the malignant cells (poorly, moderately and well-differentiated cells). The analysis of the maximum fluorescence intensity at 550 to 560 nm indicated that it was an order of magnitude higher in the case of the normal urothelial cells relative to that of any of the malignant urothelial cells (poorly, moderately and well differentiated). Finally, no statistically significant correlation could be drawn between the grade of the malignant cell types and the fluorescence intensity or the band width.

The fluorescence emission spectra of normal and tumor urothelial cells are similar to that of flavins [34]. However, the band width of normal urothelial cells is as much as 40% higher than that of malignant cells. This could indicate the contribution of an additional fluorophore emitting in the 600-nm region, the concentration of which could be higher in normal urothelial cells. Another hypothesis would be that such a difference could result from a different flavin/unbound flavin ratio [34]. This study also reveals a dramatically reduced fluorescence intensity for all malignant cell types (10 times lower), particularly in the two most undifferentiated types of TCC. This indicates that the flavin concentration may be significantly lowered in malignant urothelial cells. This observation is consistent with the early work of Pollack *et al.* [35] who showed that the flavin concentration was reduced in tumors, suggesting a "deficient" aerobic oxidation system.

Ganesan *et al.* [14] addressed the question of whether fluorescence spectroscopy can be used to identify differences in the cellular protein content of normal and malignant cells. They measured the ultraviolet fluorescence emission and excitation spectra from cultured human normal and malignant oral epithelial cell suspensions in a quartz cuvette.

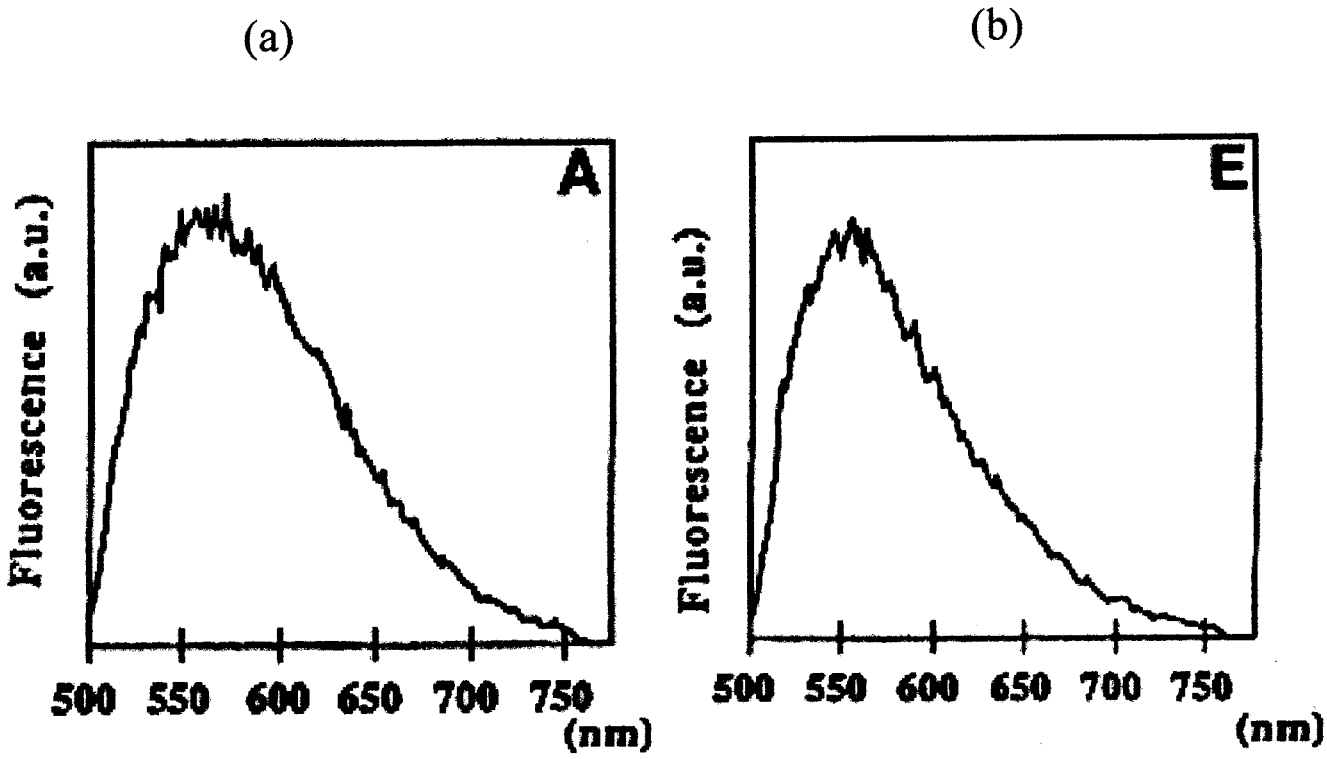

Figure 6. *Fluorescence emission spectra from (a) a normal urothelial cell and (b) a poorly differentiated transitional cell carcinoma (TCC) at 488 nm excitation.*

The fluorescence excitation spectra were measured in the range from 250 to 320 nm, for 340 nm emission and the fluorescence emission spectra were measured at 275, 285 and 310 nm excitation.

Evaluation of the normalized (to the peak intensity) excitation spectra at 340 nm emission indicates that (a) two peaks are observed near 283 and 292 nm for normal and malignant epithelial cells. The intensity of normal cells in the 250 to 289 nm spectral region is higher than that of malignant cells. The opposite is observed in the 289 to 297 nm region. An evaluation of the normalized emission spectra at 275 and 310 nm excitation indicates that, there are no differences in the line shape between normal and malignant cells. However, at 285 nm excitation, there are differences in the line shape of the spectra of these cell types.

The differences observed in the excitation spectra at 340 nm emission, between malignant and normal cells are attributed to tryptophan and tyrosine. The decreased absorption below 289 nm and increased absorption above 289 nm suggests certain conformational changes and micro-environmental changes in the amino acids.

Other groups have investigated the effect of perturbations on non-neoplastic and neoplastic cells using fluorescence spectroscopy. Specifically, Silberberg *et al.* [11] used fluorescence spectroscopy to evaluate the effect of treatment of a multicellular tumor spheroid (MTS) with the chemopreventive agent, retinoic acid. Furthermore, Zhang *et al.* [36] evaluated the effect of cellular proliferation on normal oral epithelial cell fluorescence. Finally, fluorescence spectroscopy was used to characterize terminal squamous differentiation of normal oral epithelial cells in culture [37].

Fluorescence Microscopy and Spectroscopy of Micro-Structures in Tissue Sections

Fluorescence microscopy and/or spectroscopy of fluorescent, tissue micro-structures have been performed on thin, unstained, frozen sections of a variety of tissue types, including the cervix [38], skin [39], breast [40], lung [41], aero-digestive tract [42], brain [31] and colon [15–21].

Bottiroli *et al.* [31] characterized the fluorescent micro-structures in frozen tissue sections, cut from excised specimens of the normal brain and glioblastomas using micro-spectrofluorometry. Fluorescence microscopy was performed at 366 nm excitation and at 430 or 570 nm emission. Fluorescence emission spectra were measured at 366, 405 and 436 nm excitation. Normal tissues and glioblastomas were characterized by a blue-green fluorescence with the presence of yellowish fluorescent granules. The blue-green fluorescence was less bright in the tumor than in the normal tissue section. Fluorescence emission spectra, which were measured from the micro-structures in the normal and tumor tissue sections at 366 nm excitation, were characterized by peaks at 440, 460 and 520 nm. Non-neoplastic tissues exhibited a narrow band at 440 nm and a shoulder at 460 nm. Near the tumor borderline, a slight shoulder at wavelengths longer than 500 nm became detectable. The fluorescence intensity over different emis-

sion bands was significantly decreased in the tumor region and tumor border, relative to that in the normal region. The differences in fluorescence intensity and line shape were found to be greatest at 405 nm excitation. No specific assignment was made to the micro-structures in the tumor or normal tissue sections that gave rise to the fluorescence intensity and line shape differences.

Romer *et al.* [15] characterized the fluorescent micro-structures in normal colon and colonic adenoma, frozen tissue sections using fluorescence microscopy at 351 to 364 nm excitation and 420 nm emission. The blue fibrillar fluorescence of normal tissues and adenomas arose mainly from collagen fibers in all layers of the bowel wall (mucosa, muscularis mucosae, submucosa and muscularis propria) and the yellow-amber fluorescence was attributed to eosinophil granules between the crypts in the lamina propria of the mucosa. The most important finding was the cytoplasmic, blue-green fluorescence of dysplastic epithelial cells of adenomas and the absence of such fluorescence in normal epithelial cells. This cytoplasmic fluorescence increased with increasing grade of epithelial dysplasia. The lamina propria of adenomas produced less intense collagen fluorescence than that of the normal tissue. The fluorescent eosinophilic granules were more numerous in the lamina propria of the colonic adenomas.

Wang *et al.* [16] also characterized the fluorescent micro-structures in frozen tissue sections of the normal colon, colonic adenoma and adenocarcinoma, using laser scanning confocal autofluorescence microscopy, at a similar excitation wavelength (351 to 364 nm). In the 530 to 610 nm wavelength range, a marked increase in the fluorescence intensity was observed in the dysplastic cells of adenomatous polyps, compared with normal epithelial cells. Compared to adenomatous polyps, decreased cell fluorescence was observed in adenocarcinoma. The brightest fluorescence in the lamina propria, which was attributed to eosinophils in previous studies, was also observed in other granular structures. The results reported here are in good agreement with that observed by Romer *et al.* [15].

Fairman *et al.* [17] performed confocal fluorescence microscopy of frozen tissue sections at 488 nm excitation and observed the fluorescence at wavelengths greater than 515 nm. They showed that the fluorescence of the normal mucosa originates primarily from the lamina propria, whereas in the mucosa of adenomas and hyperplastic polyps, the fluorescence was found predominantly in the epithelium. The fluorescence intensity ratio of epithelial cell to lamina propria fluorescence was significantly lower in normal mucosa, compared with adenomas and hyperplastic polyps. However, there were no statistically significant differences in the fluorescence intensity ratio of the latter two. This is in agreement with the results of Romer *et al.* [15] and Wang *et al.* [16], albeit it was performed at a different excitation wavelength.

When Izuishi *et al.* [18] performed fluorescence microscopy of frozen tissue sections at 400 to 440 nm excitation and observed fluorescence at wavelengths greater than 500 nm, they did not observe any significant difference between the fluorescence intensity of the normal mucosa and that of adenomatous and cancerous tissues of the colon. They did, however, note that in the cases where the cancer had infiltrated the submucosa, the green fluorescence due to collagen was less intense.

Bottiroli *et al.* [19] also characterized the fluorescent micro-structures in frozen tissue sections of the normal colon and colon carcinoma. However, they performed micro-spectrofluorometry, rather than fluorescence microscopy of frozen tissue sections, cut from excised specimens of normal tissues and adenocarcinoma. At 366 nm excitation, the fluorescence intensity and line shape differed between neoplastic and non-neoplastic tissues. In the non-neoplastic tissues, the fluorescence intensity at first showed a slight decrease from the superficial epithelium to the mucosa, followed by a marked increase at a depth of 450 μm, where the muscularis mucosa and the fibrous and dense connective tissue, submucosa were located. In neoplastic tissue, the fluorescence intensity as a function of depth remained relatively constant, until a depth greater than 800 μm below the surface was reached. The fluorescence emission spectra measured from non-neoplastic and neoplastic tissue differed in their spectral line shape as well. The non-neoplastic tissue section consisted of a poorly structured spectrum in the 440 to 580 nm region. The least structured line shape was observed from the submucosa, with a peak at 440 nm. A red shift of the peak position, along with a broadening of the emission band toward longer wavelengths was measured in the superficial epithelium and in the mucosa. A shoulder at about 520 nm was measured and was attributed to the presence of greenish-yellow granules. In the neoplastic tissue, the fluorescence emission spectra of the submucosal layer resembled that of similar structures in the non-neoplastic colon. The spectra of the superficial epithelium, although variable, exhibited a relatively higher intensity at longer wavelengths, relative to that of the non-neoplastic epithelium. The fluorescence emission spectra of the tumor lamina propria were characterized by the presence of an emission band at around 510 to 520 nm that appeared more evident that in the normal lamina propria. Limited areas of some sections exhibited a narrow emission band at 630 nm that can be attributed to the presence of endogenous porphyrins, possibly related to either an altered metabolism of the cancer tissue or microbial synthesis [24].

Zonios *et al.* [20] extended the efforts of Bottiroli *et al.* [19], one step further by quantifying the contribution of the fluorescent micro-structures, in frozen tissue sections to the bulk fluorescence emission spectra, measured from colon tissues, *in vivo*. To achieve this, first, fluorescence emission spectra were measured at 370 nm excitation from normal colon tissues and colonic adenomas, *in vivo*. The effect of absorption and scattering on fluorescence emission spectra measured from the tissues, *in vivo* was modeled using optical properties obtained from the analysis of Kubelka [43] of diffuse transmittance and reflectance measurements of excised human colon tissues *in vitro*. Fluorescence microscopy and micro-spectrofluorometry at 363 nm excitation, of thin, unstained, frozen tissue sections were used to

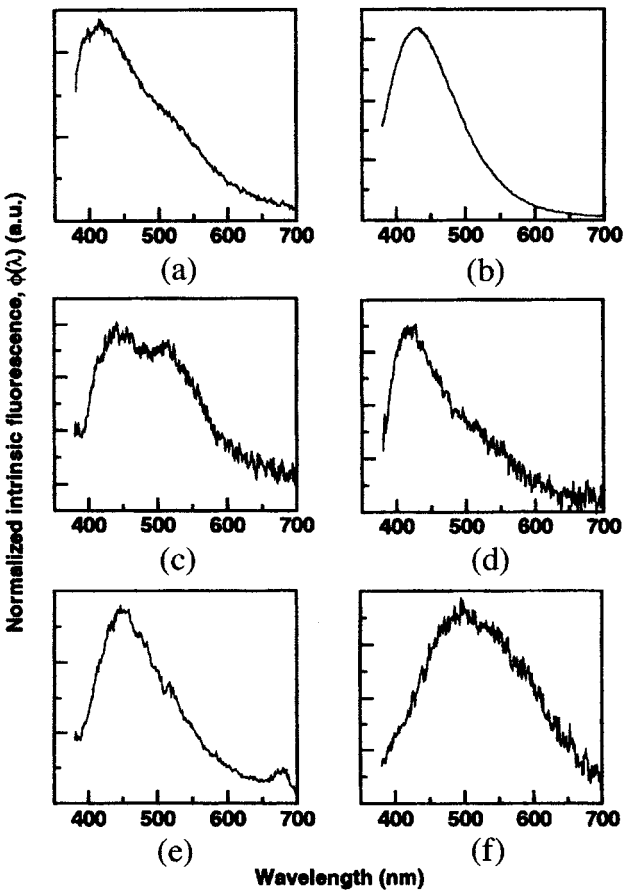

Figure 7. *Typical fluorescence emission spectra, obtained at 370 nm excitation of the various fluorescent micro-structures found in the (a) normal lamina propria, (b) adenomatous lamina propria, (c) eosinophilic granules, (d)(e) normal submucosa, and (f) dysplastic crypt cell of colon tissue.*

characterize the distribution and spectral line shapes of the fluorescent micro-structures, which contribute to the measured fluorescence emission spectrum of colonic tissues, *in vivo*. A model based on Monte-Carlo simulations [44] was used to compute the fluorescence emission spectra of colon tissues, *in vivo* using the distribution and spectral line shape of the fluorescent micro-structures and the optical properties of the excised colon tissues.

(Figure 7, *a* – *f*) shows typical fluorescence emission spectra of the various fluorescent micro-structures found in the (a) normal lamina propria, (b) adenomatous lamina propria, (c) eosinophilic granules, (d,e) submucosa, and (f) dysplastic crypt cell of colon tissue. (Figure 7, *a* and *b*) shows spectra, which are similar to that of collagen. In (Figure 7*c*), the eosinophil spectrum, exhibits a broad line shape, peaking near 520 nm in both normal and adenomatous tissues. The spectra in (Figure 7, *d* and *e*) also resemble collagen fluorescence with a peak, near 430 nm. Finally, (Figure 7*f*) shows the fluorescence emission spectrum from a typical dysplastic crypt cell, which appears to be similar to that of FAD [45].

Figure 8 shows the computed fluorescence emission spectra of normal and adenomatous colon tissue versus the corresponding average normal and adenomatous colonic tissue fluorescence spectra measured *in vivo*. The peak fluorescence intensity of the *in vivo* spectra has been scaled for comparison. The computed spectra contain all the characteristic spectral features observed in the *in vivo* spectra. The following interpretations may be made from the fluorescent micro-structures, the fluorescence density function and the transfer function used to calculate the computed fluorescence emission spectra shown in Figure 8.

1) Although the intrinsic fluorescence of collagen (the dominant fluorophore) peaks at 420 nm, the observed peak in both normal tissues and adenoma at 460 nm is due to the effect of hemoglobin absorption at 420 nm.

2) The fluorescence intensity of adenoma is smaller than that of normal colon. This is due to three factors: a) the mucosal collagen fluorescence is decreased in adenoma due to the enlargement of crypts, which displace the lamina propria, b) the submucosa contributes to the fluorescence in normal tissue but not in adenoma, because of the increased thickness of the polyp, and c) adenoma exhibits increased absorption due to hemoglobin.

3) Red fluorescence is increased in adenoma. This additional red fluorescence is primarily associated with the intrinsic fluorescence of the dysplastic crypt cells.

Zeng *et al.* [46,47] have used a similar approach to reconstruct skin fluorescence emission spectra, *in vivo*. Specifically, they measured the fluorescence emission and reflectance spectra of skin, *in vivo* and the fluorescence of the micro-structures in skin, *in vitro* [46]. The optical properties of the skin were obtained from published values in the literature. They reconstructed the fluorescence emission spectra of skin, *in vivo* using Monte Carlo simulations in which the fluorescence emission spectra and distribution of the micro-structures and the optical properties from the literature were incorporated [47]. They did not report similar reconstructions for any skin lesions, such as naevi or melanoma.

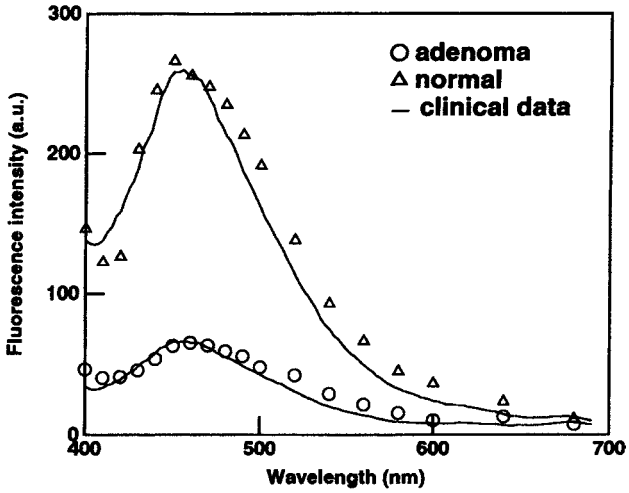

Figure 8. *The computed fluorescence emission spectra of normal and adenomatous colon tissue versus the corresponding average fluorescence emission spectra collected in vivo.*

In summary, fluorescence microscopy and spectroscopy of fluorescent micro-structures in cultured cells and frozen, tissue sections indicate that the fluorescence spectra of tissues, measured *in vivo* may be attributed to one or more of the following endogenous fluorophores: the cellular components, tryptophan, tyrosine, NADH and FAD, the structural proteins, collagen and elastin and finally, the porphyrins. Pradhan *et al.* [13] suggested that there is an increase in NADH and tryptophan, whereas Anidjar *et al.* [23] reported that there is probably a decrease in FAD, as cells progress from a non-neoplastic to neoplastic state. Romer *et al.* [15] indicated an increase in the fluorescence intensity of the dysplastic epithelial cells, when they were excited at 350 to 360 nm. This agrees with the results of Pradhan *et al.* [13]. Fairman *et al.* [17] also observed an increase in the dysplastic cell fluorescence intensity at 488 nm excitation; if this is attributed to the fluorescence of FAD, it contradicts the results reported by Anidjar *et al.* [23]. Furthermore, Bottiroli *et al.* [19] observed a red fluorescence at around 630 nm when excited at 366 nm, in some parts of neoplastic tissue sections, which they attributed to porphyrins [24]. Romer *et al.* [15] and Fairman *et al.* [17] observed a decreased fluorescence intensity from the collagen in the lamina propria of the adenomatous colon, relative to that of the normal colon. Furthermore, Izuishi *et al.* [18], Bottiroli *et al.* [19] as well as Zonios *et al.* [20] noted that because of mucosal thickening, the fluorescence of collagen from the submucosal layer in the adenomatous colon, would contribute less than that of the normal colon to the bulk tissue fluorescence emission spectrum, due to the greater attenuation of the excitation and emission light by the superficial mucosal layer in the adenoma. In addition, Zonios *et al.* [20] showed that the increased hemoglobin absorption of the adenomas also attenuates the measured fluorescence. The results of these investigations, which were performed on optically thin cells and frozen tissue sections, sets the precedent for using fluorescence spectroscopy to distinguish between optically thick, neoplastic and non-neoplastic tissues, *in vitro* and *in vivo*.

Fluorescence Spectroscopy in Animal Models

Fluorescence spectroscopy of exogenous fluorophores in tissues has been performed extensively in animal models to evaluate the uptake of photosensitizing agents for Photo Dynamic Therapy. However, only a hand full of groups has reported on fluorescence spectroscopy of endogenous fluorophores and chromophores in animal tissues. Fluorescence spectroscopy of animal models is important to consider for the following reasons. First, the progression of disease states can be studied. Second, the tissue sites can be comprehensively evaluated using different illumination and detection wavelengths, and probe geometries. Third, in addition to histologic markers, genetic and molecular markers at various stages of disease progression can also be correlated to the measured fluorescence spectra. These issues are difficult to implement in a clinical setting. The following sections survey various small animal models used for the evaluation of the diagnostic potential of fluorescence spectroscopy, and the insight they provide toward the development and application of this diagnostic technique for human tissue characterization.

Hamster cheek pouch model A well-established and reproducible animal model for fluorescence spectroscopy is the dimethylbenz[*a*]anthracene (DMBA) carcinogen-induced hamster cheek pouch model of SCC. This model mimics the biology and morphology of human oral cancer [48] and it allows for the evaluation of early neoplastic growth [49,50].

Several groups have measured fluorescence spectra of these tissues, *in vitro* [51–54] and *in vivo* [12,55–57]. Balasubramanian *et al.* [51] measured fluorescence emission spectra of normal tissues, hyperplasia, papillomas and early invasive carcinomas of the hamster cheek pouch, *in vitro* at 405 and 420 nm excitation. The fluorescence emission spectra of the transformed tissues showed peaks at 620 to 630 nm, which did not appear in normal tissues. Additionally, the fluorescence intensity at 630 nm significantly increased with disease progression. Furthermore, a ratio of the fluorescence intensity at 530 and 630 nm was determined [52]. This ratio decreased with increasing malignancy. The ratio for normal mucosa was above 3, whereas that for dysplastic tissues was less than 3. SCC had a ratio of less than one. Subsequently, Chen *et al.* [53] measured the fluorescence emission spectra of similar tissues at an excitation wavelength of 330 nm. The spectra showed two peaks at 380 and 460 nm. At 380 nm emission, the fluorescence intensity of the normal pouch was greater than those of the DMBA-treated abnormal tissues at different stages of carcinogenesis. However, at 460 nm, the converse was observed. Similar spectral differences were noted in the fluorescence emission spectra of human oral, normal and malignant tissues. Using an algorithm based on partial least squares and logistic regression to analyze the spectra at 320 nm excitation, the accuracy for identifying hyperplastic, dysplastic, early carcinomas and frankly invasive cancers was 91.7%, 83.3%, 66.7% and 83.3% [54].

Dhingra *et al.* [55] measured the fluorescence emission spectra of the DMBA-treated hamster buccal pouch model, *in vivo*, at an excitation wavelength of 410 nm. Twelve normal areas, 10 benign tissues, 20 dysplasias, four CIS and three SCCs were evaluated. The fluorescence emission spectra from the normal untreated buccal pouch in experimental animals showed two fluorescence bands, one in the blue region centered at 490 nm and a smaller band at 680 nm. Neither of these features could be correlated with histologic change. Dysplastic tissues and tissues with carcinoma, however, revealed consistently, an additional sharp peak between 630 and 640 nm [51], which was indicative of dysplasia or carcinoma. Using the ratio of fluorescence intensity at 640 and 610 nm emission wavelengths and a linear decision boundary, it was possible to correctly separate 45 of 49 histologically classified mucosal samples, with three false-positives and one false-negative result (mild dysplasia).

Van der Breggen *et al.* [56] found that fluorescence emission spectra at an excitation wavelength of 400 nm, could characterize early neoplastic transformation in the buccal mucosa of the hamster cheek pouch, but not in the adjacent buccal skin. Using a DMBA-treated hamster cheek pouch model, the fluorescence emission spectra of the buccal mucosa and the external cheek skin were measured during tissue transformation. During transformation of buccal mucosa from normal to dysplasia to carcinoma, a significant increase in the fluorescence intensity was observed. In contrast, in skin, tissue transformation was not accompanied by a change in the fluorescence intensity.

Kluftinger *et al.* [12] performed fluorescence imaging of carcinoma and dysplasia in the DMBA-induced hamster cheek pouch model at 442 nm excitation and at emission wavelengths between 480 and 520 nm (green) and above 630 nm (red). Using the criterion of a red/green ratio that is greater than 1.5 times the control, fluorescence imaging correctly identified all areas of hyperplasia (n=2), dysplasia (n=13), CIS (n=5) and invasive cancer (n=2). Eight of the 10 normal areas in the treated pouches were correctly identified as normal by a red/green ratio less than 1.5. The sensitivity and specificity of fluorescence imaging was found to be 100% and 80%. Pathak *et al.* [57] conducted a similar investigation to that described by Kluftinger *et al.* [12], and correctly identified all areas of moderate dysplasia (n=5) and severe dysplasia (n=6), two of six areas of mild dysplasia and 10 of 12 areas of normal tissue, resulting in a sensitivity of only 76%, but a similar specificity of 83%. The sensitivity difference between the current and previous investigation was attributed to the increased number of dysplasias, rather than CIS and carcinomas, in the current study.

The rat model Fluorescence spectroscopy was performed on rat tissues, which received *N*-nitrosomethyl benzylamine (NMBA), a carcinogen shown to cause esophageal malignancies [58]. Fluorescence spectroscopy of the neoplastic and non-neoplastic tissues, *in vitro* indicated that the NMBA-exposed esophageal tissues, demonstrated specific alterations in the tissue fluorescence. Specifically, the excitation spectra (at 290 and 330 nm), at 380 nm emission revealed significant differences. A corresponding change was also observed in the emission spectra (390 and 450 nm), at 340 nm excitation. At both 330 nm excitation and 390 nm emission, there was a loss of fluorescence intensity, which became pronounced as the duration of the NMBA exposure increased. This change in fluorescence correlated with the histopathological development of neoplasia in the esophageal epithelium.

Fluorescence spectroscopy was also used to study the different stages of chemically induced dysplasia and SCC of the rat palatal mucosa [59]. It was found that the epithelial dysplasia (numerically expressed in the epithelial atypia index (EAI)) of the rat palate, induced by repeated application of the carcinogen, 4-nitroquinoline 1-oxide (4NQO), showed an increase that was approximately proportional to the duration of the application period. The difference in the 670-nm fluorescence emission at 460 and 500 nm excitation showed an increase with increasing stages of epithelial dysplasia of the rat palate, suggesting that fluorescence spectroscopy has promising features for detecting dysplasia and carcinoma of the oral mucosa.

Finally, Sterenborg [60] measured fluorescence EEMs from the control ear and tumor-bearing ear (K1735P melanoma implanted intradermally) of syngenic C3H/NeN mice. The fluorescence EEMs showed broad fluorescence emission ranges, with a maximum at 365 nm excitation, and 430 to 440 nm emission. A deep valley cut through the broad fluorescence emission at 390 to 420 nm. Evaluation of the fluorescence emission spectra at 430 nm excitation of the tumor-bearing and normal ear indicated a broad fluorescence emission in the 500 to 600 nm region, a small peak at 630 nm (porhyrins), and a major peak at 670 nm (pheophorbide-a, which is food-related). Comparison of the fluorescence EEMs indicated a 40% increase in the overall fluorescence intensity in the tumors compared with the normal ears. Finally, the control ear spectra displayed dips, which are potentially due to biliverdin, oxyhemoglobin and hemoglobin. The tumor fluorescence emission spectra did not display an oxyhemoglobin dip. The results of this investigation indicate that there are differences in the fluorescence emission spectra of tumor-bearing and control tissues, *in vivo*.

Fluorescence Spectroscopy of Human Tissues

The phenomenon of fluorescence was observed first by Stokes [61]. Much later, Stubel recognized the diagnostic potential of tissue fluorescence [62]. Policard [63] observed red fluorescence when examining tumors under illumination with ultraviolet and visible light. The observed fluorescence was attributed to endogenous porphyrins in the tissue. Ghadially *et al.* [24] reported that ulcerated squamous carcinomas exhibit a red fluorescence when exposed to ultraviolet light. They concluded that this red fluorescence maybe in part due to action of bacteria on a protoporphyrin precursor. In 1965, Lycette and Leslie [64] suggested that fluorescence spectroscopy could be used to discriminate between normal tissues and malignant tumors. Fluorescence emission spectra were recorded from excised normal tissue and malignant tumors of the esophagus, stomach, breast and thyroid, at 330 nm excitation. All tissues fluoresced in the range from 360 to 600 nm. It was found that the fluorescence intensities of malignant tumors were less than that of normal tissue from the same patient. Subsequently, the groups of Profio and Doiron [65], Alfano *et al.* [66], Lohmann [67] and Yang *et al.* [68] did pioneering studies on *in vitro* and *in vivo* fluorescence spectroscopy of neoplastic and non-neoplastic, animal and human tissues.

Fluorescence spectroscopy in the ultraviolet and visible spectral regions has been developed and employed to differentiate diseased from non-diseased tissues, *in vivo*. The altered biochemical and morphologic state that occurs as tissue progresses from a non-diseased to diseased state, is reflected in the spectral characteristics of the measured

fluorescence. This spectral information can be compared to tissue histology, the current gold standard, which indicates the absence or presence and grade of disease. Mathematical algorithms can then be developed and optimized to classify tissues into their respective histologic category, based on their spectral features. These mathematical algorithms can be implemented in software, thereby potentially enabling fast, non-invasive, automated screening and diagnosis in a clinical setting.

The following section reviews the chronological evolution of fluorescence spectroscopy for various clinical applications and highlights the current status within the context of these different clinical scenarios. Specific emphasis is given to the excitation wavelength(s) used, the types of measurements that were made, the method used to dimensionally reduce the spectral variables and the corresponding classification scheme. Furthermore, the sample size for the diseased and non-diseased populations and the corresponding sensitivity and specificity are also reported. The current gold standard for the evaluation of the sensitivity and specificity of fluorescence spectroscopy is the histologic evaluation of tissue biopsies.

Currently, fluorescence spectroscopy has been employed to detect neoplastic growth in the colon, cervix, bronchus, bladder, brain, esophagus, head and neck (oral cavity, oropharynx and larynx), skin, bile duct, breast and stomach. While breast and stomach tissues have only been evaluated *in vitro*, *in vivo* studies have been performed on the other tissue sites. This may be due to the fact that the breast and stomach are not directly accessible for fluorescence spectroscopy, like the other tissues. The excitation wavelengths that have been selected to evaluate these tissues correspond to those used to excite fluorophores in the ultraviolet and visible spectral regions (see Table 1). Measurements in the form of fluorescence spectra, transient decay profiles and images have been acquired from these tissues. However, the colon is probably the only organ in which all three measurements have been performed. While fluorescence spectra and images have been measured from the bronchus, bladder, head and neck and skin, only fluorescence spectra have been measured from the cervix, brain and esophagus, thus far.

There are generally two steps involved in the development of a mathematical algorithm, which is based on fluorescence spectroscopy. The first step is to dimensionally reduce the measured spectral variables. The second step is to develop a classification scheme for the discrimination of these useful spectral parameters into relevant histologic/histo-pathological categories. The development of current mathematical algorithms based on fluorescence spectroscopy can be classified broadly into three categories: 1) algorithms based on qualitatively selected spectral variables (fluorescence intensities at several emission wavelengths), 2) algorithms based on statistically selected spectral parameters (a more robust evaluation and use of all the measured spectral information) and 3) algorithms based on parameters that reflect the biochemical and/or morphologic features of the tissue. Classification schemes employ either a binary or probability based discrimination. Mostly, algorithms have been based on qualitatively or statistically selected spectral variables in conjunction with binary classification methods.

The sensitivity is defined as the fraction of diseased samples correctly classified and the specificity is defined as the fraction of non-diseased tissues correctly classified. Although in most of the studies, the sensitivity and specificity were evaluated retrospectively, in several studies, the sensitivity and specificity were evaluated prospectively to obtain an unbiased estimate of the performance of the technique under consideration [33,69–77]. In some studies, the sensitivity and specificity were evaluated for a combination of fluorescence spectroscopy and conventional endoscopy [33,75]. Finally, in the case of tissues such as the bladder, larynx, skin, breast and stomach, the sensitivity and specificity were reported for the discrimination between cancers and non-cancers, only. This is different from other studies in which the sensitivity and specificity were reported for the discrimination of cancers and *pre-cancers* from normal tissues. In the majority of studies performed, the sensitivity and specificity are greater than 80% reflecting the high classification accuracy of fluorescence spectroscopy for the detection of neoplastic tissues, *in vivo*. The sensitivity and specificity reported appear to be comparable to or superior to current clinical modalities that are routinely used.

Colon Several groups have evaluated fluorescence spectroscopy for the identification of human colonic neoplasms *in vitro* [78–82] and *in vivo* [32,69,83–90]. Both steady-state and time-resolved, fluorescence measurements as well as fluorescence imaging have been evaluated at multiple excitation wavelengths.

Richards-Kortum *et al.* [78] measured fluorescence emission spectra from normal colon tissues and adenomatous colonic polyps, *in vitro* at a range of excitation wavelengths, spanning the ultraviolet and visible spectrum. They found that the spectral differences between normal and adenomatous colon tissues were greatest at 330, 370 and 430 nm excitation. Furthermore, at an excitation wavelength of 370 nm, fluorescence intensities at 404, 480 and 680 nm were found to be most useful for differentiating adenomas from normal colon tissues. Kapadia *et al.* [79] obtained fluorescence emission spectra from 35 normal specimens and 35 adenomatous polyps of the colon at 325 nm excitation. They used multivariate linear regression analysis of the spectra and a binary classification scheme to develop and optimize an algorithm that differentiates adenomatous polyps from normal mucosa and hyperplastic polyps, retrospectively. The algorithm prospectively discriminated 16 adenomatous polyps from 16 hyperplastic polyps and 34 normal tissues, with a sensitivity of 100% and specificity of 98%. Yang *et al.* [80] evaluated the ratio of the fluorescence intensities at two emission wavelengths, from fluorescence emission spectra at 325 nm excitation and at two excitation wavelengths, from fluorescence excitation spectra at 450 nm, emission of 35 colon adenocarcinomas and 39 normal

colon specimens. An algorithm based on the simple ratio of fluorescence intensities and a linear decision surface separated adenocarcinomas from normal tissues with a sensitivity and specificity of greater than 90%. Finally, Chwirot *et al.* [81] measured fluorescence images in six spectral bands at 325 nm excitation from 50 resected specimens of the colon. For the majority of neoplastic lesions, the fluorescence intensity was lower than that of corresponding normal mucosa in all of the spectral bands. The spectral bands centered at 440 nm and 475 nm seemed the most promising.

Schomacker *et al.* [83] measured fluorescence emission spectra from 86 normal sites, 35 hyperplastic polyps and 49 adenomatous polyps of the colon, *in vivo* at 337 nm excitation. Multivariate linear regression analysis and a binary classification scheme was used to differentiate spectra of hyperplastic and adenomatous polyps and resulted in a sensitivity and specificity of 86% and 80%, respectively. These values were not significantly different from the accuracy of routine clinical pathology. In a subsequent report, Schomacker *et al.* [84] also examined the fluorescence emission spectra of 86 normal sites, 35 hyperplastic polyps, 49 adenomatous polyps and seven adenocarcinomas of the colon, obtained both *in vitro* and *in vivo* at 337 nm excitation. The spectra of colonic tissue measured *in vivo* and *in vitro* were different, primarily due to NADH fluorescence, which decays exponentially with time after resection. Again, using a similar method of analysis, adenocarcinoma and adenoma were distinguished from hyperplastic and normal tissues with a sensitivity and specificity of 80% and 92%, respectively. Adenocarcinoma and adenomatous polyps were distinguished from hyperplastic polyps with a sensitivity and specificity of 86% and 77%, respectively. Eker *et al.* [85] also measured the fluorescence emission spectra from 32 adenomas, 114 hyperplastic polyps of the colon, *in vivo* at 337 nm excitation. Stepwise multivariate linear regression and a binary classification scheme yielded a sensitivity and specificity of 100% and 84%, respectively, for discriminating adenomas from hyperplastic tissues and normal mucosa.

Cothren *et al.* [86] obtained fluorescence emission spectra at 370 nm excitation from 31 adenomas, four hyperplastic polyps and 32 normal sites of the colon, *in vivo*. They developed an algorithm for differentiating adenomas from normal and hyperplastic tissues based on 1) a drop in the maximum fluorescence intensity at 460 nm and 2) a relative increase in the red fluorescence intensity at 680 nm, which occurred as tissue progressed from normal to hyperplasia to adenoma. Using these spectral features in a Bayesian classification scheme, they could differentiate adenomas from normal mucosa and hyperplastic polyps with a sensitivity and specificity of 100% and 97%, respectively. Another interesting application of fluorescence spectroscopy was presented by Catalano *et al.* [87]. They collected fluorescence emission spectra at 370 nm excitation from the rectal mucosa of 16 patients with a history of adenomatous polyps (within the last 18 months) and from 16, age and gender matched patients with no such history. Polyp formers had an increased fluorescence intensity at 680 nm compared with non-polyp formers. However, differences in the spectra were small and no hypothesis was stated suggesting a predictive capability of this technique for identifying patients with colorectal mucosa at risk for developing colorectal neoplasia.

In their most recent report, Cothren *et al.* [69] developed a probability based algorithm based on fluorescence intensities at several emission wavelengths for the detection of colonic adenomas and evaluated it in a blinded manner. Fluorescence emission spectra were acquired at an excitation wavelength of 370 nm, from 91 normal tissues, 19 hyperplastic polyps and 62 adenomatous polyps, *in vivo*.

(Figure 9*a*) displays fluorescence emission spectra obtained at 370 nm excitation from normal mucosa, a hyperplastic polyp and an adenomatous polyp from a typical

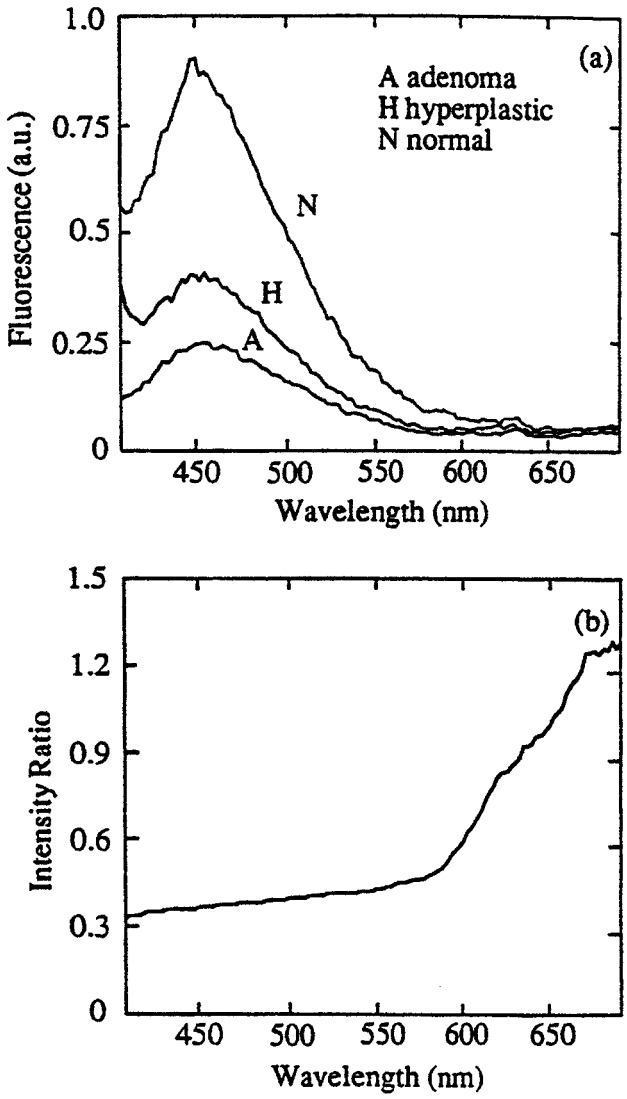

Figure 9. *(a) Fluorescence emission spectra obtained in vivo at 370 nm excitation from normal mucosa, a hyperplastic polyp and an adenomatous polyp from the colon of a typical patient and (b) the ratio of the mean adenomatous polyp fluorescence spectrum divided by the mean normal fluorescence spectrum.*

patient. Each exhibits strong fluorescence near 460 nm and weak fluorescence at wavelengths greater than 600 nm. Generally, the peak fluorescence intensity of normal mucosa is greater than that of adenomatous polyps, with hyperplastic polyps, intermediate in intensity. These differences were consistent within a patient. The ratio of the mean adenomatous polyp spectrum divided by the mean normal spectrum is shown in (Figure 9*b*). The flat area near 460 nm indicates a region in which the shapes of both spectra are similar, but where the fluorescence intensity of the normal mucosa is three times as intense as that of the adenoma. The rising curve beyond 600 nm shows the existence of additional structure in the red region of the adenoma spectra.

A calibration data set was used to develop and optimize an algorithm to differentiate tissue types based on probability distributions of the fluorescence intensity at 460 nm and the ratio of the intensities at 680 and 600 nm. Evaluation of the algorithm on the calibration data set containing 44 normal mucosa, 12 hyperplastic polyps and 35 adenomas indicated a sensitivity of 94% and a specificity of 91% for differentiating adenoma from hyperplastic and normal tissues. The algorithm was then tested in a blinded fashion on a prediction data set. Evaluation of the algorithm on the prediction data set, which contained 50 normal mucosa, 17 hyperplastic polyps and 32 adenomas indicated a similar sensitivity and specificity of 90% and 88%, respectively, for differentiating adenomas from hyperplastic polyps and normal mucosa.

Wang *et al.* [88] demonstrated the use of endoscopic fluorescence imaging to identify dysplasia associated with adenomatous polyps in the colon. Endoscopic white light and fluorescence images at 351 to 364 nm excitation and >400 nm emission, were collected using a video colonoscope from a polyp in an area that covered approximately 80% of that illuminated by the white light (total fluorescence image is 150×150 pixels, which corresponds to a region which is 3.5×3.5 cm^2). In total, 12 adenomas and six hyperplastic tissues were evaluated.

Single-point fluorescence intensity measurements obtained from fluorescence imaging are shown in Table 2. The fluorescence intensity of normal mucosa was approximately a factor of two greater than that of adenomatous polyps. The intensity of the hyperplastic polyps and that of normal mucosa were similar. Also, foci of dysplasia were distinguished from those of hyperplasia, suggesting that the basis of dysplasia identification was determined by factors other than gross morphology of the polyp. Blood vessels showed a 25% reduction in intensity, relative to corresponding normal mucosa. Mucosal folds were found to cast shadows that also resulted in reduced fluorescence intensity. The shadows were more prominent on fluorescence than on white light images. Twelve adenomatous polyps were identified with a sensitivity of 83%. Because additional biopsy specimens were not obtained from normal appearing colonic mucosa in this study, no comment was made regarding the specificity of this technique.

Table 2. Single-point, Fluorescence Intensity Measurements (Mean ± Standard Deviation) Obtained *In Vivo* at 351 to 364 nm Excitation and >400 nm Emission, from 12 Adenomas, Six Hyperplastic Polyps and Six Blood Vessels and the Corresponding Normal Tissue Site in the Colon.

Fluorescence intensity	Adenoma	Hyperplastic	Blood vessels
Corresponding normal	100 ± 27.5	100.0 ± 18.1	100.0 ± 16.1
Left of polyp	54 ± 16.3	87.9 ± 16.3	75.3 ± 5.1
Center of polyp	59.9 ± 16.7	95.9 ± 16.7	
Right of polyp	54.4 ± 17.7	98.1 ± 17.7	

In addition to the work conducted by Wang *et al.* [88], preliminary reports [89,90] of real-time fluorescence imaging with blue light excitation and a false-color display of the relative red and green fluorescence intensities have demonstrated that flat adenomatous lesions in the colon that were not visible by white light endoscopy (WLE) could be detected. Furthermore, hyperplastic polyps could be distinguished from adenomatous polyps. However, the sensitivity and specificity were not reported.

Unlike the previous groups, Mycek *et al.* [32] explored the feasibility of making time-resolved, rather than steady-state, fluorescence measurements from the colon, *in vivo* and assessed the sensitivity and specificity of this technique for distinguishing adenomatous polyps from non-adenomatous polyps. Time-resolved, fluorescence measurements were obtained *in vivo* from the colon at 337 nm excitation and 550 nm emission (40 nm band pass), with a time resolution of 4.8 nsec. Seventeen patients with a total of 13 adenomatous and 11 non-adenomatous (six hyperplastic, three mucosal prolapse, one lymphoid aggregate, one aberrant crypt focus) polyps were studied.

(Figure 10, *A* and *B*) shows (a) representative fluorescence decay profiles of an adenomatous polyp and (b) the normalized profiles (to a peak intensity of 1), which reveal identical fluorescence decays between two different measurements. From these curves, the transient decay time was characterized by measuring the time interval between 0.2 of the normalized fluorescence intensity at the rising edge of the curve and at the decaying portion of the curve. For the two polyp groups, the mean value of the decay time was found to be 9.3 ± 0.4 nsec for adenomatous polyps and 10.5 ± 0.7 nsec for non-adenomatous polyps. By choosing a threshold of 9.8 nsec, the adenomatous polyps were distinguished from non-adenomatous polyps with a sensitivity of 85% and specificity of 91%. The accuracy of the time-resolved fluorescence technique is comparable to the accuracy of routine clinical pathology, which is approximately 87% as noted in two previous studies [69,83].

Table 3 summarizes the results of the clinical investigations performed thus far, on fluorescence spectroscopy of the colon, *in vivo*. The table indicates: (1) the excitation wavelengths, (2) the measurement type, (3) the emission wavelengths of the fluorescence intensities used and the corresponding decision scheme, (4) the sample size for the non-diseased (ND) and diseased (D) tissue categories and finally, (5) the resulting sensitivity (SE) and specificity (SP) for differentiating adenomas (A) and/or adenocarcinomas (C) from hyperplasia (H) and/or normal tissue (N). Evaluation of Table 3 indicates that the two primary

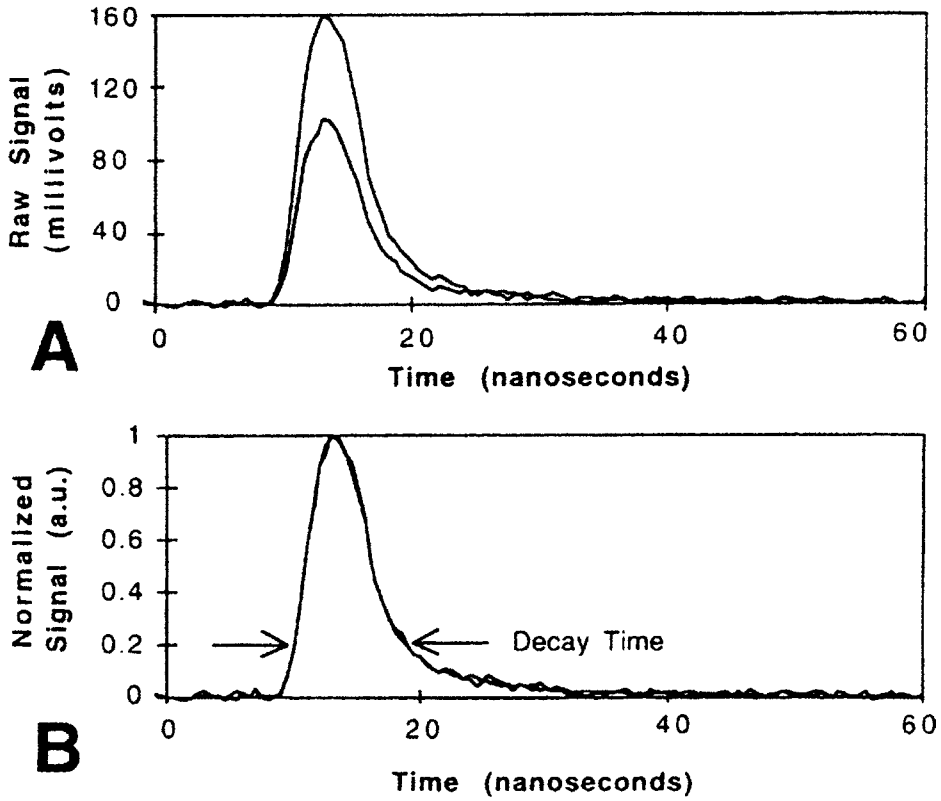

Figure 10. *(A) Representative fluorescence decay profiles of an adenomatous polyp and (B) the normalized profiles (to a peak intensity of one), which reveal identical fluorescence decays between two different measurements.*

excitation wavelengths used were 337 and 370 nm excitation. All of the groups, except for two, measured fluorescence emission spectra. Of the remaining two, one measured fluorescence images [88], whereas the other measured the transient fluorescence decay from colon tissues [32], *in vivo*. Either the entire fluorescence emission spectra (at 337 nm excitation) or fluorescence intensities at a few emission wavelengths (at 370 nm excitation) were used as the spectral discriminators. A binary classification scheme was used in all cases, except for one (in which a Bayesian probability based classification scheme was used) [69]. Furthermore, in all of the studies performed, except for one, the performance of fluorescence spectroscopy was evaluated retrospectively. Only Cothren *et al.* [69] used a calibration and prediction data set, respectively, to develop and test their technique, in an unbiased manner. The sensitivity and specificity for differentiating adenocarcinoma/adenoma from hyperplastic and normal tissues ranged from 80% to 100%, with no dramatic differences resulting from for the measurement type, excitation wavelength, emission wavelength or method of analysis used.

Table 3. A Summary of Results Obtained by Several Groups on Fluorescence Spectroscopy of the Colon, *In Vivo*. The Table Indicates: 1) the Excitation Wavelengths, 2) the Measurement Type, 3) the Emission Wavelengths of the Fluorescence Intensities Used and the Decision Scheme, 4) the Sample Size for the Non-diseased (ND) and Diseased (D) Tissue Categories and Finally, 5) the Resulting Sensitivity (SE) and Specificity (SP) for Differentiating Adenomas (A)/Adenocarcinomas (C) from Hyperplasia (H) and/or Normal Tissue (N).

Group	Excitation wavelength (nm)	Measurement type	Dimension reduction: emission wavelengths (nm)	Classification: decision scheme	Sample size ND; D	SE; SP (%)
Schomacker *et al.*, 1992b [84]	337	Spectra	MVLR (Spectra)	Binary	N(86), H(36); A(49), C(7)	80; 92
Eker *et al.*, 1999 [85]	337	Spectra	MVLR (Spectra)	Binary	N(68), H(114); A(32)	96; 84
Cothren *et al.*, 1990 [86]	370	Spectra	*I* (460, 680)	Binary	N(32), H(4); A(31)	100; 97
Cothren *et al.*, 1996 [69]	370	Spectra	*I* (460, 600, 680 nm)	Bayes theorem	N(50), H(17); A(32)	90; 88*
Schomacker *et al.*, 1992a [83]	337	Spectra	MVLR (Spectra)	Binary	H (35); A(49)	86; 80
Schomacker *et al.*, 1992b [84]	337	Spectra	MVLR (Spectra)	Binary	H(36); A(49), C(7)	86; 77
Wang, 1999 [88]	360	Images	*I* (>400 nm)	Binary	H(6); A(12)	83; N/A
Mycek *et al.*, 1998 [32]	337	Decay	τ (550 nm)	Binary	H(13), A(11)	85; 87

I, intensity; τ, decay time; *MVLR*, multivariate linear regression.
*Sensitivity and specificity were evaluated retrospectively and prospectively.

Cervix Several groups have explored the utility of detecting cervical neoplasia, *in vitro* using fluorescence spectroscopy [91–94]. However, Richards-Kortum and coworkers [70–72,95–102] have done the most extensive development and evaluation of fluorescence spectroscopy for the detection of cervical neoplasia, *in vivo*. All of the efforts have focused on the measurement of single-pixel, fluorescence emission spectra from cervical tissues at multiple excitation wavelengths.

Lohmann *et al.* [91] first investigated the utility of fluorescence emission spectra at 365 nm excitation, for the recognition of cervical neoplasia, *in vitro*. They found that the spectra of the cervix exhibited a single peak with a maximum at 475 nm. The fluorescence intensity increased, with the degree of increase proportional to the degree of dysplasia. In contrast, the fluorescence intensity of carcinoma was very small, with a rise in intensity at the border between the carcinoma and normal tissue. Glassman *et al.* [92,93] measured fluorescence emission spectra of normal tissues and gynecological tissues with carcinoma, *in vitro* at 300 and 320 nm excitation. Consistent differences were seen in the fluorescence intensity of carcinoma and normal tissues from all sites. Mahadevan *et al.* [94] demonstrated that the greatest spectral differences in the fluorescence emission spectra of non-neoplastic and neoplastic cervical tissues, *in vitro* occur at 340, 380 and 460 nm excitation. Koumantakis *et al.* [103] studied the fluorescence emission spectra of malignancies in the female genital tract, *in vivo*, including the ovaries, fallopian tube, uterus and cervix uteri, using 442 nm excitation and concluded that this could enhance selective detection of malignant tissue, and thereby reduce the risk of leaving it untreated.

Richards-Kortum and coworkers have developed multivariate algorithms, based on fluorescence emission spectra at multiple excitation wavelengths for the detection of cervical dysplasia [97,98]. They have tested these algorithms retrospectively and prospectively on diagnostic [70] and screening [72] populations. Furthermore, they have evaluated the safety of using fluorescence spectroscopy relative to standard procedures, such as colposcopy [99]. Also, they have evaluated the effect of acetic acid, cervical mucus and vaginal medications on the fluorescence emission spectra [100]. Finally, they have constructed receiver-operator curves (ROC) for fluorescence spectroscopy, standard clinical screening and diagnostic tests and competing technologies, to evaluate the performance of each for the detection of cervical dysplasia [101]. Finally, they have performed a cost analysis to demonstrate the potential of a diagnostic technique, such as fluorescence spectroscopy to reduce health care costs in the detection of cervical dysplasia [102]. The following paragraphs provide a more detailed discussion of these various studies.

Initially, Ramanujam *et al.* [95] collected fluorescence emission spectra *in vivo* from 114 cervical tissue sites from a group of 28 patients at 337 nm excitation. A two-stage algorithm based on empirically selected spectral parameters demonstrated that it is feasible to discriminate between low grade squamous intraepithelial lesions (SILs) and normal epithelia as well as between high grade SILs and low grade SILs. Subsequently, Ramanujam *et al.* [97,98] expanded their efforts to measure fluorescence emission spectra from the cervix at multiple excitation wavelengths. Specifically, tissue spectra from 40 patients at 337 and 380 nm excitation and from 24 patients at 337 and 460 nm excitation demonstrated that spectra at multiple excitation wavelengths provide better discrimination between dysplastic and non-dysplastic tissues.

In the most recent report, Ramanujam *et al.* [70] obtained fluorescence emission spectra at all three excitation wavelengths (337, 380 and 460 nm) from a total of 186 normal squamous tissues, 27 normal columnar tissues, 29 tissues with inflammation, 47 low grade SILs and 70 high grade SILs in 95 patients. A multivariate statistical algorithm was developed for the differential detection of SILs and particularly, high grade SILs. There were four primary steps involved in the multivariate statistical analysis of tissue spectra. The first step was to pre-process spectra to reduce inter-patient and intra-patient variation within a tissue type. The pre-processed spectra were then dimensionally reduced to an informative set of principal components, which describe most of the variance of the original spectral data set using Principal Component Analysis (PCA). Next, the principal components, which contain diagnostically relevant information, were selected using an unpaired, one-sided student's *t*-test. Finally, a classification scheme based on Bayes theorem was developed using these diagnostically relevant principal components.

Inputs into the multivariate statistical algorithm included the pre-processed fluorescence emission spectra at all three excitation wavelengths (full-parameter) and fluorescence intensities at a select, reduced number (15) of excitation-emission wavelength pairs (reduced parameter) selected from the component loadings of the principal components. The algorithm was developed on a calibration set and then tested on a prediction set with an approximately equal number of samples in each tissue category. The prospective sensitivity and specificity of the full-parameter, multivariate statistical algorithm for differentiating SILs from non-SILs was 82% and 68%, respectively. This algorithm differentiated high grade SILs from non-high grade SILs prospectively, with a sensitivity and specificity of 79% and 78%, respectively. The sensitivity and specificity of the reduced-parameter algorithm, which uses an order of magnitude fewer variables was within 5% of that reported for the full-parameter algorithm. This suggests that fluorescence intensities at a reduced number of optimal, excitation-emission wavelength pairs, rather than the entire fluorescence emission spectra can be measured and employed for the detection of cervical dysplasia.

Subsequent to this analysis, a neural-networks-based classification scheme, which replaces the steps involving PCA and Bayes theorem was developed [71]. This algorithm used the pre-processed fluorescence intensities at the 15 excitation-emission wavelength pairs (inputs into the reduced-parameter, multivariate statistical algorithm) as

inputs into a radial basis function network ensemble to classify the different tissue types. Again, the algorithm was optimized on a calibration set and tested on a prediction set of approximately equal prior probability. The prospective sensitivity and specificity of the neural-networks-based algorithm for differentiating SILs from non-SILs were 91 ± 1.5% and 67 ± 0.75%, respectively. The similarity in the performance of the linear (multivariate statistical algorithm) and non-linear (neural networks) methods of analysis provided confidence in the results obtained from this clinical investigation.

In a subsequent investigation, Brookner *et al.* [72], measured cervical tissue fluorescence emission spectra at 337, 380 and 460 nm excitation from 54 women who had not had an abnormal Pap smear, previously (screening population). These were compared to previously reported results from 95 patients, all of whom had abnormal Pap smears (diagnostic population) [70]. Before fluorescence spectroscopy in the screening population, a Pap smear was performed on each woman. The results indicated an abnormal finding in only four of the 54 women evaluated. In the 50 women with normal Pap smears, spectra were measured from a total of 186 sites; of these, 103 contained normal squamous tissues, 23 contained normal columnar tissues and 60 were from the transformation zone. In the four women with abnormal Pap smears, spectra were measured from 16 sites; eight contained squamous tissue, one contained columnar tissue and seven were from the transformation zone.

Classification of the normal tissue fluorescence emission spectra using the previously developed multivariate statistical algorithm [70] indicated that 87% of normal squamous tissues and 78% of tissues from the transformation zone were correctly classified. Furthermore, 76% of normal columnar tissues were correctly classified. Hence, even though the multivariate statistical algorithm had been developed for a population in a diagnostic setting, its performance was robust in a screening setting as well.

Brookner *et al.* [99] also examined the photochemical risks associated with the detection of human cervical dysplasia using fluorescence spectroscopy. In particular, they compared the relative risk of fluorescence spectroscopy to colposcopy (a procedure in which a low power microscope is routinely used to illuminate the cervix for evaluation). They measured the average wavelength-dependent spectral radiant exposure (J/cm^2 per nanometer) during a colposcopic examination and during fluorescence spectroscopy of the cervix. To quantify the relative risk, they multiplied these illumination spectra by several action spectra (efficacy of photochemical damage as a function of wavelength) from the literature and compared the areas under the curve, corresponding to each procedure. Based on this comparison, they concluded that risks of illumination for fluorescence spectroscopy are lower than or comparable to those already encountered in routine diagnostic procedures such as colposcopy.

Agrawal *et al.* [100] explored the fluorescence properties of several substances commonly found on the cervix: acetic acid, cervical mucus, and vaginal medications. Acetic acid is routinely used during colposcopy, to enhance visual differences between normal and abnormal areas of the cervix. Areas, which may develop into cervical cancer, undergo a transient whitening visible to the naked eye. Cervical mucus is often present on the ectocervix as well as in the fold of the endocervical canal. During colposcopy, attempts are made to remove this mucus from the cervix to improve visualization of the tissue, but complete removal can be difficult. Vaginal medications are commonly used for the treatment of yeast and other infections.

The results of this investigation showed that acetic acid introduces changes in both the line shape and intensity of fluorescence emission measured from the cervix, at 337 nm excitation. Specifically, the application of acetic acid caused a decrease in the fluorescence intensity of dysplastic and non-dysplastic tissues. However, the dysplastic tissues displayed a greater decrease in the fluorescence intensity. At emission wavelengths, below 500 nm, acetic acid caused a greater percentage of patients to exhibit differences between dysplastic and non-dysplastic tissue in their fluorescence emission spectra. At emission wavelengths above 500 nm, acetic acid provided no appreciable enhancement. The measured mucus transmission demonstrated strong protein absorption below 300 nm. In general, no significant absorption bands were observed in the visible part of the spectrum. The mucus fluorescence intensity was strongest at 280 nm excitation and 340 nm emission (tryptophan). Weaker fluorescence intensities could be observed at 350 nm excitation, 450 nm emission (NADH) and at 450 nm excitation, 535 nm emission (FAD). In examining the spectra of the 16 medications, 10 of them had clear fluorescent peaks, whereas six of the agents exhibited very broad fluorescent peaks or no recognizable peak at all. In summary, while acetic acid enhances fluorescence spectroscopy of dysplastic and non-dysplastic cervical tissues, cervical mucus and vaginal medications that produce strong fluorescence, could interfere with these measurements.

Mitchell *et al.* [101] described ROC curves for fluorescence spectroscopy, which were generated from fluorescence spectroscopy in a diagnostic setting [70] and compared them with ROC curves for other diagnostic methods (colposcopy, Pap smear, cervicography, speculoscopy, HPV testing), which were calculated from published reports.

Summary ROC curves were developed from independent reports of the sensitivity and specificity of each test. Furthermore, the area under the curve (AUC) and the *Q* point on the ROC curve (at which the sensitivity equals the specificity) were calculated. Evaluation of these features indicated that fluorescence spectroscopy outperformed the other tests, but most importantly, compared favorably with colposcopy, the current standard diagnostic technique for cervical neoplasia.

Finally, Cantor *et al.* [102] compared five strategies for the diagnosis and treatment of cervical SILs, including those that incorporate colposcopy and fluorescence spectroscopy.

On the basis of a health care perspective, they performed a cost-effective analysis using a decision-analytic model for the diagnosis and management of SILs. They compared the five strategies based on expected costs and number of cases that were treated appropriately, missed, treated inappropriately and appropriately not treated in a hypothetical cohort of 100 patients referred after an abnormal Pap smear. Data on prevalence and operating characteristics were derived from the medical literature. Costs were adjusted from hospital charge data. A see-and-treat strategy based on fluorescence spectroscopy was the least expensive, but also the least effective strategy, costing US$160,479 to detect 31.55 cases of SIL accurately in 100 patients. The most expensive strategy was colposcopically directed biopsy, at US$311,808 to find 45.78 cases; however, when both tests were used in a see-and-treat strategy modality, slightly more cases were found (46.05) at a lower cost (US$285,133).

Bronchus Lam and coworkers [33,104–110] have developed and evaluated fluorescence emission spectra and subsequently, fluorescence images at two emission wavelengths for the detection of invasive carcinoma, CIS and dysplasia of the bronchus and lung, *in vivo*. This work has resulted in a commercial, laser induced fluorescence endoscopy (LIFE) device (Xillix Technologies Corporation, Richmond, BC, Canada). The LIFE device has been tested in a multi-center clinical trial to evaluate if fluorescence bronchoscopy when used as an adjunct to white light bronchoscopy (WLB) can improve the bronchoscopist's ability to locate areas suspicious of dysplasia for biopsy and histologic examination. The LIFE device has also been successfully used to evaluate neoplastic lesions in other organ sites, including the larynx [75,76,111], gastrointestinal tract [89,90], head and neck [73,74] and the bile duct [77].

Originally, Hung *et al.* [104] measured the bronchial fluorescence emission spectra of 32 patients with severe dysplasia, CIS and invasive carcinoma at 405, 442 and 488 nm excitation, *in vivo*. The spectra at 405 and 442 nm excitation, were similar to each other, with two peaks at 520 and 590 nm. Furthermore, the spectra of normal and neoplastic tissues showed similar line shapes at these excitation wavelengths. However, the intensity decreased as tissue progressed from normal to severe dysplasia to CIS to invasive cancer. Palcic *et al.* [105] subsequently developed an endoscopic-based fluorescence bronchoscope that provided simultaneous white light images and pseudo-color images based on the ratio of the fluorescence intensity in the green and red wavelength bands, at 442 nm excitation (basis for the design of the LIFE device). Lam *et al.* [108] evaluated 53 patients with known bronchogenic carcinoma and 41 volunteers, using conventional WLB and the fluorescence bronchoscope described previously [105]. They showed that the two techniques had a similar specificity of 94%. However, the sensitivity of fluorescence bronchoscopy (73%) was 50% greater than that of WLB (48.4%) for detecting dysplasia and CIS.

Most recently, Lam *et al.* [33] evaluated if fluorescence bronchoscopy with the LIFE device when used as an adjunct to WLB could improve the bronchoscopist's ability to locate areas suspicious of dysplasia for biopsy and histologic examination. A multi-center trial was conducted in seven institutions in the United States and Canada. WLB followed by fluorescence bronchoscopy with the LIFE device was performed in 173 patients known or suspected to have lung cancer. The histologic diagnosis for a total of 700 biopsy specimens were as follows: 321 normals; hyperplasia, metaplasia or mild dysplasia in 237; moderate/severe dysplasia in 93; CIS in nine and invasive carcinoma in 40. Thus, a total of 142 biopsy specimens were graded as moderate dysplasia or worse, a total of 102 biopsy specimens were graded as moderate/severe dysplasia or CIS and a total of 40 biopsy specimens were graded as invasive carcinoma. This was then used as the standard to determine the relative sensitivity of the bronchoscopic procedure.

A three-point classification system was used for WLB evaluation. Areas without any visual abnormality were classified as class 1. Areas with non-specific erythema, swelling or thickening of the bronchial mucosa, bronchoscopic trauma, anatomic anomalies or granulation tissue were classified as class 2. Nodular/polypoid lesions, irregularity of the bronchial mucosa, or focal thickening of the subcarina, suspicious for high grade dysplasia or carcinoma were labeled as class 3. In fluorescence bronchoscopy, green images were considered normal and class 1, areas that were slightly brown with ill-defined margins were labeled as class 2 and brownish/red images were considered as class 3. The physician's bronchoscopic classification was converted from a three-point scale to a two-point scale in which classes 1 and 2 were considered negative and class 3 was considered positive.

On a lesion-by-lesion analysis, WLB alone had a sensitivity of 24.6% for detecting moderate dysplasia or worse. With the addition of fluorescence bronchoscopy, the sensitivity increased to 66.9%. On a per patient basis, the sensitivity of WLB for detecting individuals harboring at least one lesion was 37.3%. With the addition of fluorescence bronchoscopy, the sensitivity increased to 75%. On a lesion-by-lesion basis, WLB had a sensitivity of 8.8% for detecting moderate/severe dysplasia or CIS. The addition of fluorescence bronchoscopy increased the sensitivity to 56%. Finally, WLB had a sensitivity of 65% for detecting invasive carcinoma. WLB + LIFE improved this to a sensitivity of greater than 90%. It should be noted that the addition of fluorescence bronchoscopy added an average of 13.8 minutes to a conventional WLB, which took an average of 9.4 minutes. No adverse events related to the use of this device were observed.

Bladder Several groups [27,112–115] have measured single-pixel, fluorescence emission spectra at different excitation wavelengths from invasive carcinoma, early carcinoma and dysplasia of bladder tissues, *in vivo*.

D'Hallewin *et al.* [112] evaluated the fluorescence emission spectra of normal and neoplastic urothelium,

including CIS at 365 and 355 nm excitation. The line shape of the fluorescence emission for CIS and TCC were identical to that of normal bladder tissue. However, the fluorescence intensity of CIS was lower than that of normal tissues (average decrease of 2.6 times), with TCC exhibiting the weakest fluorescence intensity (average decrease of 3.2 times). Using this spectral information, they demonstrated that fluorescence emission spectra at 365 nm excitation can be used to discriminate between normal bladder, CIS and TCC, *in vivo* with high accuracy.

Baert *et al.* [113] measured fluorescence emission spectra of the bladder at 337 and 405 nm excitation. Using 337 nm excitation, the ratio of the fluorescence intensities at 460 and 400 nm was used to differentiate successfully between normal urothelium and visible papillary bladder carcinoma. Using 405 nm excitation, the fluorescence intensity for some cases of dysplasia was lower than that of normal tissue. However, this was not consistent.

Koenig *et al.* [114] explored the applicability of fluorescence spectroscopy for the detection of bladder carcinoma. Fluorescence emission spectra at 337 nm excitation were measured from a total of 35 sites with inflammation (24 chronic and 11 acute), 42 normal areas, one squamous metaplasia, seven dysplasias, 28 carcinomas and one CIS.

The fluorescence intensity of the normal urothelium was 20 times greater than that of carcinoma in the human bladder. Inflammatory tissues also showed weak fluorescence, but there were significant spectral differences between these and carcinoma. While inflammatory tissues and normal tissues had two fluorescence maxima at 385 and 455 nm, the typical spectrum of the carcinomas showed only one maximum at 455 nm. Using the ratio of fluorescence intensities at 385 and 455 nm, and a binary decision scheme, carcinoma was discriminated from non-carcinomas with a sensitivity and specificity of 97% and 98%, respectively. Differentiation of dysplastic bladder lesions from normal urothelium was not possible. Furthermore, no significant differences in spectra could be detected between the different stages (T1 or T3) or grades (1 to 3) of carcinoma.

More recently, Koenig *et al.* [27] performed an investigation in which they measured fluorescence emission spectra at 337 nm excitation from suspicious (erythematous, edematous, raised and so forth) bladder lesions and areas from which random biopsies were obtained during routine cystoscopy. They also measured epithelial thickness in all biopsy samples to determine whether it correlates with the spectra, measured *in vivo*. Spectra at 337 nm excitation were measured during cystoscopy from a total of 130 bladder areas in 17 women and 58 men in whom bladder carcinoma was suspected. A total of 23 and 107 biopsies, respectively, were obtained from areas with and without carcinoma. The ratio of the fluorescence intensities at 385 and 455 nm was determined for every measured area and correlated with histologic results and epithelial thickness. Using the ratio parameter in a binary decision scheme, 95% of carcinomas were correctly classified and only 30 non-carcinomas were classified as false-positives. This suggests that the number of non-cancerous areas biopsied during routine white light cystoscopy would be reduced from 107 to 30 (72% fewer) if fluorescence spectroscopy was used to guide biopsy. Furthermore, the ratio of the fluorescence intensity at 385 and 455 nm was found to decrease exponentially with increasing epithelial thickness between 1 and 225 μm. Beyond 225 μm, there was no further ratio decay indicating that most of the measured fluorescence originates from the uppermost 225 μm of the epithelium.

Anidjar *et al.* [115] investigated the ability of fluorescence spectroscopy to distinguish urothelial bladder carcinoma from normal or non-specific inflammatory mucosa. Fluorescence emission spectra were acquired from 22 normal mucosa, 13 sites with nonspecific inflammation, five sites with CIS and 26 invasive cancers at 480, 337 and 308 nm excitation.

At 480 nm excitation, the fluorescence emission spectrum has a peak at 580 nm. The fluorescence intensity of inflammatory tissues was decreased compared to that of normal mucosa. The intensity was decreased further for all bladder carcinomas, including CIS. At 337 nm excitation, the

Table 4. A Summary of Results Obtained by Several Groups on Fluorescence Spectroscopy of the Bladder, *In Vivo*. The Table Indicates: 1) the Excitation Wavelengths, 2) the Measurement Type, 3) the Emission Wavelengths of the Fluorescence Intensities Used and the Decision Scheme, 4) the Sample Size for the Non-diseased (ND) and Diseased (D) Tissue Categories and Finally, 5) the Resulting Sensitivity (SE) and Specificity (SP) for Differentiating Carcinoma from Dysplastic, Inflammatory and Normal Tissues.

Group	Excitation wavelength (nm)	Measurement type	Dimension reduction: emission wavelengths (nm)	Classification: decision scheme	Sample size ND; D	SE; SP (%)
D'Hallewin *et al.*, 1994 [112]	365	Spectra				
	355					
Baert *et al.*, 1993 [113]	337	Spectra	*I* (460,400)	Binary		
	365					
Koenig *et al.*, 1996 [114]	337	Spectra	*I* (385, 440)	Binary	85; 29	97; 98*
Koenig *et al.*, 1998 [27]	337	Spectra	*I* (385, 440)	Binary	107; 20	95; 72.5*
Anidjar *et al.*, 1996b [115]	308	Spectra	*I* (360, 440)	Binary	31; 35	100; 100*
	337					
	480					

I, intensity.
*Sensitivity and specificity were calculated for the discrimination between cancers and non-cancers (other investigations calculated the sensitivity and specificity for discriminating pre-cancers and cancers from normal tissues).

fluorescence emission spectra had a peak at 450 nm. Similar changes in the fluorescence intensity were observed at 337 nm excitation as was observed at 480 nm excitation. At 308 nm excitation, the fluorescence emission spectra of normal mucosa consisted of one broad band of fluorescence with two secondary maxima at 380 and 440 nm. The spectra of tumors differ markedly from that of normal mucosa, since the two distinct fluorescence bands were shifted to 360 and 440 nm. Furthermore, the ratio of the fluorescence intensities at 360 and 440 nm increased significantly as tissue progressed from normal to inflammation to carcinoma. Using this diagnostic parameter and a binary decision scheme, a 100% sensitivity and specificity was achieved for the detection of bladder carcinoma.

Table 4 summarizes the results obtained by the aforementioned groups on fluorescence spectroscopy of the bladder, *in vivo*. The table indicates that spectra were acquired from these tissues at a range of excitation wavelengths from 300 to 500 nm. However, only spectra at 308, 337 and 365 nm excitation were analyzed for the purpose of developing classifiers. In all the cases, the ratio of fluorescence intensities at two emission wavelengths was used in a linear decision scheme to discriminate between carcinomas and non-carcinomas. These algorithms retrospectively discriminated between these two tissue types, with a sensitivity that was close to 100% and a specificity that ranged from 70% to 100%.

Brain Two groups have reported on the measurement of fluorescence emission spectra from brain tissues, *in vitro* and *in vivo*. Montan and Strombland [116] examined the fluorescence emission spectra at 337 nm excitation of neoplastic and non-neoplastic brain tissue, *in vivo* during a craniotomy and *in vitro* following tissue preservation by freezing or formaldehyde. They reported that meningiomas, but not astrocytomas differed from normal, white and gray matter. Preservation by freezing, significantly altered both the fluorescence line shape and intensity, whereas formaldehyde fixation did not affect spectral line shape, but did affect the fluorescence intensities.

Bottiroli *et al.* [31] performed a preliminary investigation to evaluate if fluorescence spectroscopy can be used for intra-operative delineation of tumor resection margins in the brain. Fluorescence emission spectra at 366 nm excitation were measured from the brain cortex, white matter and neoplastic lesion of three patients with glioblastoma. In the cases evaluated, the fluorescence intensity of the glioblastoma was significantly lower than that of the white matter. A reduction in fluorescence intensity, although to a lesser extent, was observed in the glioblastomas, relative to the cortex tissues in two of the three patients. Compared with normal tissues, the glioblastoma spectra also showed a red-shift in the peak fluorescence emission.

Esophagus Single-pixel, steady-state, fluorescence emission spectra have been measured from Barrett's esophagus, esophageal cancer and normal tissues, *in vivo*. Originally, Panjehpour *et al.* [117] and Vo-Dinh *et al.* [118] measured fluorescence emission spectra of normal and cancerous tissue during endoscopy in patients with esophageal cancer and in cancer free volunteers at 410 nm excitation. Multiple fluorescence measurements were obtained from 32 patients including measurements from 123 normal areas and 36 esophageal cancers. Using a classification model based on linear discriminant analysis, esophageal cancers were classified with a sensitivity and specificity of 100% and 98%, respectively.

Subsequently, Panjehpour *et al.* [119] described the use of endoscopic fluorescence spectroscopy at 410 nm excitation to detect high grade dysplasia in patients with Barrett's esophagus. In 36 patients, a total of 216 spectra were obtained from non-dysplastic Barrett's mucosa, 36 spectra were obtained from mucosa with low grade dysplasia, 10 spectra were obtained from tissues with high grade dysplasia and 46 spectra were obtained from mucosa with low grade dysplasia and focal high grade dysplasia.

The normalized fluorescence emission spectrum of a non-dysplastic Barrett's mucosa was characterized by a broad band emission with a peak at around 500 nm. A comparison between the normalized spectra of the non-dysplastic and dysplastic mucosa indicated that the latter is significantly lower in intensity and slightly red shifted. A mathematical model based on differential normalized fluorescence was developed and the fluorescence intensities at 480 and 660 nm were selected as the spectral variables. Discrimination was achieved using a binary decision scheme. The sensitivity and specificity of fluorescence spectroscopy for discriminating high grade dysplasia from low grade dysplasia and normal tissues was 40% and 96%, respectively. However, when the spectra were re-evaluated per patient, the sensitivity and specificity increased to 100% and 76%, respectively. It should be noted that erosive esophagitis contributed to an increase in the false-positive rate. Hence, further studies are required to determine if this technique can correctly classify tissues with inflammation.

Head and neck— oral cavity Several groups have investigated the utility of fluorescence measurements for detecting invasive carcinoma, early carcinoma and dysplasia of head and neck tissues, *in vitro* [120–122] and *in vivo* [73,74, 123–127]. Both fluorescence spectra and images have been evaluated.

Ingrams *et al.* [120] compared the fluorescence emission spectra from a total of 12 normal (healthy mucosa or benign lesions) and 10 abnormal (dysplastic or carcinoma) tissue samples, *in vitro* at multiple excitation wavelengths between 250 and 500 nm. Significant spectral differences were observed between the two groups, with the greatest differences observed at 410 nm excitation and 635 nm emission. Majumder *et al.* [121] measured the fluorescence emission spectra of normal and cancerous oral tissues at 300, 337 and 460 nm excitation. They found that the integrated fluorescence intensity at 337 nm excitation was higher in normal tissues, relative to that in cancerous tissues. These differences were not observed at 300 and 460 nm excitation. Yang *et al.* [122] also measured fluorescence

emission spectra at multiple excitation wavelengths (280, 290, 300, 320, 330, 340 nm) for distinguishing between cancerous and normal mucosal tissues, *in vitro*. They found that by using ratios of intensities at specific emission wavelengths, at the short and long excitation wavelengths in a binary decision scheme, they were able to achieve a sensitivity of 81.25% and a specificity of 93.75%.

Kolli *et al.* [123] were the first to measure fluorescence excitation and emission spectra from normal mucosa and neoplastic lesions of the oral cavity in 31 patients, *in vivo*. They found that the fluorescence properties of the neoplastic mucosa were significantly different from those of normal mucosa when excited with UV light in the 200 to 340 nm range.

Dhingra *et al.* [124] characterized the fluorescence emission spectra of healthy and diseased oral mucosa and oropharynx, *in vivo* at 370 and 410 nm excitation. Fluorescence emission spectra were obtained from normal mucosa (n=5), hyperplasia and hyperkeratosis (n=8), lichen planus (n=1), dysplasia (n=4), CIS (n=1) and invasive SCC (n=5).

All fluorescence emission spectra exhibited a single broad peak centered at 450 and 490 nm with excitation wavelengths of 370 and 410 nm, respectively. At 410 nm excitation, the neoplastic tissues displayed a decreased blue intensity and increased red intensity relative to non-neoplastic and normal tissue. These spectral differences were much less dramatic at 370 nm excitation. The fluorescence intensities at 490 and 640 nm emission (excitation wavelength, 410 nm), were normalized to the corresponding intensity at the contralateral normal site from the same patient. These were then incorporated into a simple binary decision algorithm to differentiate neoplastic tissues from non-neoplastic and normal tissues with a sensitivity and specificity of 100% and 87.5%.

Gillenwater *et al.* [125] evaluated fluorescence spectroscopy for the detection of oral cavity neoplasia, *in vivo* at 337, 365 and 410 nm excitation. A total of 27 sites in 10 patients were evaluated and histology indicated that 17 sites were normal and 11 sites had dysplasia or carcinoma.

In general, the peak fluorescence intensities of abnormal sites were less than those of normal sites. The fluorescence intensities of abnormal sites were increased in the red spectral region compared with those of normal sites. Although differences were noted at all three excitation wavelengths, the fluorescence intensity at 337 and 410 nm excitation provided the best discrimination between normal and abnormal tissues. An algorithm was developed to discriminate dysplasia and carcinoma from normal mucosa using two variables, which exploit these spectral differences. These were the peak intensity at 337 nm excitation and the ratio of the intensities in the red (635 nm) and blue (490 nm) regions at 410 nm excitation (red-blue peak ratios). To account for inter-patient variation, the ratio of the peak intensity at 337 nm excitation of the normal and abnormal spectra was calculated. Also, the ratio of the red-blue peak ratios at 410 nm excitation for abnormal and normal tissues was calculated. Using these two parameters in a binary classification algorithm, carcinoma and dysplasia could be differentiated from normal tissues with a sensitivity and specificity of 94.1% and 100%, respectively. Clinical impression had a lower sensitivity and similar specificity of 76.5% and 100%.

With respect to fluorescence imaging of head and neck tumors, Kulapaditharom and Boonkitticharoan [73] aimed to: 1) test whether the LIFE device (Xillix Technologies) described previously for fluorescence bronchoscopy [33] could correctly identify sites of cancer in the head and neck and 2) to compare the performance of LIFE and WLE for cancer detection. Thirty-two examinations with LIFE and WLE were performed in 25 patients with signs and/or symptoms suggesting cancers in the head and neck (larynx, oral cavity and tracheobronchial tree). Pre-treatment and post-treatment investigations with LIFE and WLE were conducted to see whether LIFE correctly reflects the treatment effects as defined by clinical and histologic findings. Biopsies were performed at spots in which positive findings were suggested by either or both imaging modalities. Random biopsies were obtained in cases where both techniques revealed negative findings.

In evaluating 16 cancerous lesions and 16 non-cancerous lesions, LIFE had a sensitivity and specificity of 100% and 87.5%, respectively, whereas WLE had a sensitivity of 87.5% and a specificity of only 50%. Both imaging techniques encountered certain cases of false-positives. Inflammatory masses and granuloma were the causes. A comparison of WLE and LIFE for evaluating treatment response in six patients indicated that LIFE was considered to be more reliable (accuracy 93.8%) than WLE (accuracy 69%) for differentiating diseased from non-diseased tissue.

Kulapaditharom and Boonkitticharoan [74] also used fluorescence imaging with the LIFE device to determine the effectiveness of detecting unknown primary cancers in the head and neck. Thirteen patients with biopsy-proven cervical node metastases were evaluated prospectively with the LIFE device and panendoscopy. Among the 13 positive sites identified by the LIFE device, histopathology confirmed five as SCC, four as dysplasia, two as inflammation and two as normal. Panendoscopy with random biopsy located only two lesions. In summary, the LIFE device and panendoscopy localized unknown primary cancers at rates of 38.5% and 15.4%. The LIFE device not only aided in revealing a greater proportion of occult primary cancers, but also helped in reducing the number of unnecessary biopsies.

Betz *et al.* [127] evaluated normal and malignant mucosa in patients with head and neck cancer through measurements of both fluorescence images and fluorescence emission spectra. Specifically, fluorescence images were acquired at 375 to 440 nm excitation and >515 nm emission on a total of 30 patients. Fluorescence emission spectra were acquired using the same excitation band from a healthy volunteer and a total of 36 patients. Evaluation of the results indicated that in 13 of the 30 patients (43.3%), tumors were distinguished from their normal surroundings through a reduction of the green fluorescence intensity. However, spectral analysis indicated that the peak fluorescence

intensity at 511 nm was lower in tumors relative to that of normal mucosa in 34 of the 36 patients. The spectral line shape of the tumors did not differ markedly from that of normal mucosa.

Head and neck — larynx There have been several reports on steady-state, fluorescence measurements and imaging of laryngeal cancers, *in vivo* [75,76,111]. In 1995, Harries *et al.* [111] acquired fluorescence emission spectra at 442 nm excitation, from normal and pathologically confirmed tissues of the larynx in eight patients, *in vivo*. They also acquired fluorescence images using the LIFE device (Xillix Technologies), which is described previously for fluorescence bronchoscopy [33]. The results suggested that the fluorescence properties of laryngeal tissue are similar to those of bronchial tissue and that the LIFE device has the potential to increase the accuracy of cancer staging in the larynx.

Zargi *et al.* [75,76] determined the role of fluorescence imaging for the detection of laryngeal cancer. Fluorescence laryngoscopy of the red and green fluorescence intensities at 442 nm excitation was performed using the LIFE device (Xillix Technologies) [33] in 40 patients [75]. Histopathology of 115 biopsy specimens proved 28 sites to be positive and 87, negative for malignancy. While laryngomicroscopy alone had a sensitivity and specificity of 60% and 83%, respectively, the combination of laryngomicroscopy and fluorescence laryngoscopy had a sensitivity and specificity of 85% and 87%, respectively. In a subsequent investigation [76], Zargi *et al.* evaluated the effect of keratosis on microlaryngoscopy and fluorescence laryngoscopy in 30 patients. After histopathology, 22 sites were identified as malignant and 72 sites were identified as benign. For clinical sites that included keratosis, microlaryngoscopy had a sensitivity and specificity of 54% and 86%, respectively. The sensitivity and specificity of the LIFE device was 59% and 76%, respectively. For tissues without keratosis, microlaryngoscopy had a sensitivity and specificity of 50% and 86%, respectively, whereas LIFE had a sensitivity and specificity of 56% and 75%, respectively. Keratosis, which emits a strong fluorescence, can give a false impression of a malignant process, hence reducing the specificity of fluorescence imaging.

Table 5 summarizes the results of the clinical investigations performed thus far, on fluorescence spectroscopy of the head and neck, *in vivo*. Evaluation of Table 5 indicates that a variety of excitation wavelengths between 337 and 440 nm have been used. Both fluorescence emission spectra and images have been measured. Note that in all cases, fluorescence intensities or ratios of intensities at several emission wavelengths were used in conjunction with a binary classification scheme. While most of the algorithms were evaluated only retrospectively, some were evaluated prospectively as well [73–76]. The sensitivity and specificity for differentiating neoplastic from non-neoplastic oral cavity tissues ranged from 85% to 100%, except in the investigation conducted by Betz *et al.* [127], where fluorescence imaging resulting in a significantly lower sensitivity than fluorescence spectroscopy. The sensitivity and specificity for differentiating laryngeal cancers from the normal larynx was poor for fluorescence imaging alone [75,76], but increased substantially when it was combined with microlaryngoscopy [75]. It should be noted that in all studies except those reported by Dhingra *et al.* [124] and Gillenwater *et al.* [125], the sensitivities and specificities are reported for the discrimination between cancers and non-cancers.

Skin There have been mixed reports on the diagnostic potential of fluorescence spectroscopy and imaging for skin melanomas, *in vivo*. The first attempt at using fluorescence spectroscopy for the detection of melanoma, *in vivo* was made by Lohmann [67]. They excited healthy skin tissues, naevi and melanomas at 365 nm excitation and recorded the

Table 5. A Summary of Results Obtained by Several Groups on Fluorescence Spectroscopy of the Head and Neck, *In Vivo*. The Table Indicates: 1) the Excitation Wavelengths, 2) the Measurement Type, 3) the Emission Wavelengths of the Fluorescence Intensities Used and the Decision Scheme, 4) the Sample Size for the Non-diseased (ND) and Diseased (D) Tissue Categories and Finally, 5) the Resulting Sensitivity (SE) and Specificity (SP) for Differentiating Carcinoma and Dysplasia from Inflammatory and Normal Tissues.

Group	Excitation wavelength (nm)	Measurement type	Dimension reduction: emission wavelengths (nm)	Classification: decision scheme	Sample size ND; D	SE; SP (%)
Dhingra *et al.*, 1996 [124]	370	Spectra	*I* (490)	Binary	14; 10	100; 87.5
	410		*I* (640)			
Gillenwater *et al.*, 1998a [125]	337	Spectra	*I* (peak)	Binary	17; 11	94; 100
	410		*I* (635, 490)			
Kulapaditharom and Boonkitticharoan, 1998a [73]	442	Images	*I* (red, green)	Binary	16; 16	100; 87.5*‡
Betz *et al.*, 1999 [127]	375 – 440	Images, Spectra	*I* (>515 nm)	Binary	36; N/A	43.3; N/A‡
					36; N/A	94.4; N/A‡
Harries *et al.*, 1995 [111]	442	Images	*I* (red, green)	Binary		
Zargi *et al.*, 1997a [75]	442	Images	*I* (red, green)	Binary	87; 28	85; 87*†‡
Zargi *et al.*, 1997b [76]	442	Images	*I* (red, green)	Binary	72; 22	59; 76*‡

I, intensity.
*Sensitivity and specificity were evaluated prospectively.
†Sensitivity and specificity were evaluated for a combination of fluorescence and conventional endoscopic techniques.
‡Sensitivity and specificity were calculated for the discrimination between cancers and non-cancers (other investigations calculated the sensitivity and specificity for discriminating pre-cancers and cancers from normal tissues).

corresponding fluorescence emission spectra. They found that the spectra had a peak at 475 nm. The fluorescence intensity was very low for melanoma, compared to that of normal skin tissue, and there was a local increase in the intensity in a transition zone between the melanoma and areas of healthy skin, followed by a drop in the intensity measured for the latter. Such local maxima were not found for the naevi. When the above hypothesis was tested in a larger group of 147 patients [128], it was found that the ratio of the fluorescence intensity at 470 nm outside and within the pigmented lesions was substantially higher for the melanomas compared with naevi.

However, these reports [67,128] were not confirmed by Sterenborg *et al.* [129]. They measured fluorescence, EEMs of normal skin and human skin carcinomas *in vivo* at excitation wavelengths ranging from 375 to 600 nm. They found no correlation between either the line shape or the intensity of the fluorescence emission and histopathology of the tissue. They concluded that fluorescence spectroscopy is not a feasible diagnostic technique for melanomas.

However, Chwirot *et al.* [130] used fluorescence imaging for the detection of melanomas, *in vivo* at 365 nm excitation and 475 nm emission, as was done by Lohmann [67] and Lohmann *et al.* [128], with moderate success. Fluorescence images were obtained for 90 patients with melanomas of different forms and stages, 169 patients with 205 pigmented naevi and 105 patients with 113 skin lesions of different types, hereafter referred to as others.

Healthy skin was characterized by a relatively homogeneous distribution of fluorescence intensity. The fluorescence images of melanoma showed inhomogeneous spatial distributions of intensity, both within the lesions and around them. Ratios of maximum fluorescence intensity measured for regions located up to 40 mm from the lesions, to a minimum fluorescence intensity within the lesions, were useful for the detection of melanomas. Using this ratio in a binary classification scheme, the sensitivity and specificity for differentiating melanoma from naevi and other skin lesions was 82.5% and 78.6%, indicating that fluorescence imaging is indeed a feasible diagnostic technique for melanomas.

Bile duct Thus far, there has only been one report on fluorescence imaging of bile duct cancer, *in vivo* [77]. In this pilot investigation, nine patients with bile duct cancer underwent percutaneous, transhepatic, fluorescence cholangioscopy using the LIFE-GI (Xillix Technologies) device, described previously for fluorescence bronchoscopy [33]. Fluorescence images in the red and blue wavelength emission bands were obtained at 437 nm excitation. Histologic confirmation was performed with surgically resected specimens or biopsy specimens. Under observation of the fluorescence cholangioscope, normal mucosa was seen as light blue, whereas cancerous lesions were observed as irregular and heterogeneous dark red areas. Additionally, in seven of nine patients, a white color (strong fluorescence) was seen. It corresponded to the region of abundant fibrous stroma in the cancerous lesion. This white fluorescence (which may reflect the saturation of detector) reflects the enriched fibrous stroma, which is exposed to the internal lumen as a result of cancer filtration.

Breast tissues Several groups have evaluated the fluorescence excitation and emission spectra for breast cancer detection, albeit, this has been done only on tissues, *in vitro*. Alfano *et al.* [131] measured the fluorescence emission spectra of normal and malignant breast tissues *in vitro* from two patients at 488 nm and at 457.9 nm excitation. Normal and malignant tissues both showed a peak at about 515 nm, while the normal tissue also exhibited additional maxima at 556 and 592 nm. Yang *et al.* [132] obtained fluorescence excitation and emission spectra of normal, malignant and adipose breast tissues, *in vitro*. They were able to distinguish malignant tissue from adipose glandular fibrous and normal tissue with a sensitivity of 91% (56 malignant tissues) and a specificity of 95% (46 benign/normal tissue specimens). Furthermore, three ratios of fluorescence intensities at different wavelengths in the excitation spectrum over the 250 to 320 nm range, for 340 nm emission, in conjunction with a binary decision scheme, yielded a sensitivity and specificity of 90% to differentiate 103 malignant tissues from 63 benign/normal tissues [133]. Gupta *et al.* [134] compared the fluorescence emission spectra of benign (fibroadenoma, 35 patients), cancerous (ductal carcinoma, 28 patients) and normal tissues, *in vitro* at 337 nm excitation. The fluorescence intensity, which was integrated over the entire emission wavelength range, was increased in cancerous tissues, relative to that in benign and normal tissues. Using this variable in a linear decision algorithm, cancerous tissues were discriminated from benign and normal tissues with an accuracy of 100%. Lohmann and Kunzel [40] found that the fluorescence emission spectra of breast tissue at 340 to 380 nm excitation was associated primarily with connective tissue fibers in between lactiferous ducts and lobular complexes.

Stomach tissues Chwirot *et al.* [135] presented the first and only report on fluorescence imaging of stomach cancers, *in vitro*. Specifically, they measured fluorescence images of 21 resected specimens of stomach cancers and normal tissues, *in vitro* at six visible wavelengths, at 325 nm excitation. Using the fluorescence intensities at 440 nm and 395 nm, normalized to that at 590 nm and a linear decision surface, cancerous tissues were classified with a sensitivity of 96%.

Conclusions and Future Perspectives

In summary, fluorescence spectroscopy has been demonstrated as a powerful diagnostic technique for the detection of neoplastic growth in a variety of epithelial tissue sites. The high sensitivity and specificity of this technique coupled with its fast and non-invasive detection capability can render it useful in both a screening and diagnostic setting. Most of the studies to date have focused on steady-state measurements of fluorescence emission spectra from small tissue regions.

However, the now commercial LIFE device (Xillix Technologies), which was originally used for fluorescence bronchoscopy and which is now being extended to other tissue sites, is an example of the successful application of fluorescence imaging. The use of time-resolved, fluorescence measurements for the characterization of neoplastic and non-neoplastic tissues, *in vivo* has just begun to evolve.

To improve the role of fluorescence spectroscopy in clinical oncological applications, several issues have yet to be addressed fully. Evaluation of the clinical investigations performed within and between different tissue sites indicates that there is a considerable variability in the implementation of this technology. In particular, the variability arises in the selection of excitation and emission wavelengths, probe geometry and the method of analysis of the spectral information. This is especially evident from the review of clinical investigations reported in this paper.

To select the optimal excitation and emission wavelengths, it is necessary to be able to measure the fluorescence of tissues, at multiple excitation and emission wavelengths in the ultraviolet and visible spectral regions. This has been performed extensively to characterize tissue fluorescence *in vitro* using a conventional laboratory spectrofluorometer [9]. Due to the use of an excitation and emission monochromator in this instrument, measurement times, for an entire fluorescence EEM can take as long as an hour, and clearly is impractical in a clinical setting. Fluorescence spectroscopy of tissues, *in vivo*, has mostly been performed at one, two or three excitation wavelengths, using single-pixel fluorometers, which incorporate a pulsed excitation light source, a fiber-optic probe, a spectrograph and an intensified photo diode array. Recently, Zangaro *et al.* [136] elaborated on this basic design to enable the measurement of fluorescence at multiple excitation-emission wavelengths (fluorescence EEMs) and diffuse reflectance spectra of tissues, *in vivo*. Rapid excitation wavelength tunability was achieved by mounting dye cuvettes (with appropriate dyes, which are capable of generating excitation light at multiple wavelengths) on a rotating wheel that rapidly traverses a single resonant cavity of a laser. Also, a corresponding filter wheel placed in front of the spectrograph, which when synchronized with the dye wheel allowed rejection of back-scattered, excitation light at each wavelength. Fluorescence EEMs could be measured from colon tissues in less than a second with this instrument. Subsequently, Zuluaga *et al.* [137] also developed a fast, EEM system that measures fluorescence emission spectra at multiple excitation wavelengths and diffuse reflectance spectra, rapidly (4 minutes total measurement time) and non-invasively from tissues, *in vivo*. The primary difference between this system and that developed by Zangaro *et al.* [136] is that it employs a white light source with a series of band pass filters, instead of a nitrogen pumped-dye laser for generating multiple excitation wavelengths for fluorescence spectroscopy.

The optimization of the probe geometry and the method of analysis has been limited somewhat by the fact that the underlying biochemical and morphologic features that give rise to differences in the fluorescence measured from neoplastic and non-neoplastic tissues has not been rigorously quantified for all tissue types. Zonios *et al.* [20] made perhaps the first attempt to measure and quantify the biochemical and morphologic basis of neoplastic and non-neoplastic colonic tissue fluorescence emission spectra measured, *in vivo* and made several interesting findings as discussed previously in this review. Investigations such as these are essential to identify the diagnostically fluorescent micro-structures that contribute to the tissue fluorescence emission spectra and the optimal probe geometry that can maximally exploit these features.

Animal models are useful with regard to developing methodologies that can be used to elucidate the biochemical and morphologic properties of tissue and optimizing the instruments to exploit these features. The advantages they offer are: 1) they are well-established, 2) spectral measurements can be made per tissue site for a variety of experimental and biologic conditions and 3) data can be obtained from a statistically significant number of animals for the purpose of validation, without the need for expensive clinical trials.

Most screening and diagnostic algorithms developed from fluorescence spectroscopy of tissues incorporate qualitatively or statistically selected spectral variables, which are evaluated using a binary or probability based classification scheme. For example, Panjehpour *et al.* [119] have developed an algorithm, which uses qualitatively selected, fluorescence intensities at several emission wavelengths in a binary classification scheme, for the detection of Barrett's esophagus, *in vivo*. Nevertheless, Ramanujam *et al.* [70] have developed an algorithm, which uses statistically selected spectral variables and probability based classification for cervical pre-cancer detection, *in vivo*. This multivariate statistical algorithm employs PCA to dimensionally reduce pre-processed, tissue fluorescence emission spectra into orthogonal principal components, with minimal information loss. Bayes theorem is then used to develop probability based classification using the diagnostically relevant, principal components. The advantage of using statistical rather than qualitative analysis of the tissue fluorescence emission spectra is that the entire spectral information content can be exploited. Furthermore, the benefit of using a probability, rather than a binary classification scheme is that the likelihood of the classification being correct is also provided. In spite of the obvious advantage of using a statistically based evaluation of the spectral parameters, the clinical investigations in this review indicate that both methods appear to provide similar classification accuracy, within the various clinical contexts evaluated, thus far. Hence, this suggests that fluorescence intensities at only a few emission wavelengths may carry most of the diagnostically relevant information that is needed to discriminate between diseased and non-diseased tissues. Another point to note regarding screening and diagnostic algorithms is that very few groups prospectively evaluated the performance of their fluorescence spectroscopy based algorithms. This is surprising given the fact that it is

necessary to have training and test data sets to really evaluate the performance of an algorithm in an unbiased manner.

With respect to clinical applications, the diagnostic potential of fluorescence spectroscopy is defined by histology. To evaluate if fluorescence spectroscopy is sensitive to changes that precede the morphologic manifestations seen by histologic evaluation, it is valuable to correlate the measured spectral information to other biochemical and/or genetic markers of increased cancer risk. Furthermore, although fluorescence spectroscopy has been most widely explored for the detection of pre-cancer or cancer in a screening and diagnostic setting, its diagnostic potential for guiding surgery has only been evaluated in a limited number of clinical studies [31]. Because this technique can discriminate between diseased and non-diseased tissues, in a fast and non-invasive manner, it could be used to define margins of resection for various surgical procedures, such as that of the breast and brain. Additionally, this technique could also be used to monitor the response of tissues to various therapeutic interventions.

Acknowledgements

The author gratefully thanks Mary Leonard for her extensive help with the preparation of the figures for this manuscript.

References

[1] Wagnieres GA, Star WM, and Wilson BC (1998). *In vivo* fluorescence spectroscopy and imaging for oncological applications. *Photochem Photobiol* **68** (5), 603–632.

[2] Richards-Kortum R, and Sevick-Muraca E (1996). Quantitative optical spectroscopy for tissue diagnosis. *Annu Rev Phys Chem* **47**, 555–606.

[3] Andersson-Engels S, Johansson J, Stenram U, Svanberg K, and Svanberg S (1990). Malignant tumor and atherosclerotic plaque diagnosis using laser induced fluorescence. *IEEE J Quantum Electron* **26** (12), 2207–2217.

[4] Andersson-Engels A, Johansson J, Svanberg K, and Svanberg S (1991). Fluorescence imaging and point measurements of tissue: applications to the demarcation of malignant tumors and atherosclerotic lesions from normal tissue. *Photochem Photobiol* **53** (6), 807–814.

[5] Andersson-Engels S, and Wilson BC (1992). *In vivo* fluorescence in clinical oncology: fundamentals and practical issues. *J Cell Pharmacol* **3**, 66–79.

[6] Papazoglou TG (1995). Malignancies and atherosclerotic plaque diagnosis— Is laser induced fluorescence spectroscopy the ultimate solution? *J Photochem Photobiol B: Biol* **28**, 3–11.

[7] Bigio IJ, and Mourant JR (1996). Ultraviolet and visible spectroscopies for tissue diagnostics: fluorescence spectroscopy and elastic-scattering spectroscopy. *Phys Med Biol* **42**, 803–814.

[8] Andersson-Engels S, Klinteberg CA, Svanberg K, and Svanberg S (1997). *In vivo* fluorescence imaging for tissue diagnostics. *Phys Med Biol* **42**, 815–824.

[9] Lakowicz JR (1983). *Principles of Fluorescence Spectroscopy*. Plenum Press, New York.

[10] Campbell ID, and Dwek RA (1984). *Biological Spectroscopy*. Benjamin/Cummings Publishing Co., Menlo Park, CA.

[11] Silberberg MB, Savage HE, Tang GC, Sacks PG, Alfano RR, and Schantz SP (1994). Detection of retinoic acid induced biochemical alterations in squamous cell carcinoma using intrinsic fluorescence spectroscopy. *Laryngoscope* **104** (3 Pt 1), 278–282.

[12] Kluftinger AM, Davis NL, Quenville NF, Lam S, Hung J, and Palcic B (1992). Detection of squamous cell cancer and pre-cancerous lesions by imaging tissue autofluorescence in the hamster cheek pouch model. *Surg Oncol* **1**, 183–188.

[13] Pradhan A, Pal P, Durocher G, Villeneuve L, Balassy A, Babai F, Gaboury L, and Blanchard L (1995). Steady state and time resolved fluorescence properties of metastatic and non-metastatic malignant cells from different species. *J Photochem Photobiol B: Biol* **31** (3), 101–112.

[14] Ganesan S, Sacks PG, Yang Y, Katz A, Al-Rawi M, Savage HE, Schantz SP, and Alfano RR (1998). Native fluorescence spectroscopy of normal and malignant epithelial cells. *Cancer Biochem Biophys* **16**, 365–373.

[15] Romer TJ, Fitzmaurice M, Cothren RM, Richards-Kortum R, Sivak MV, Jr., and Kramer JR, Jr. (1995). Laser-induced fluorescence microscopy of normal colon and dysplasia in colonic adenomas: implications for spectroscopic diagnosis. *Am J Gastroenterol* **90** (1), 81–87.

[16] Wang H, Willis J, Canto MJF, Sivak MV, Jr., and Izatt JA (1999). Quantitative laser scanning confocal autofluorescence microscopy of normal, premalignant, and malignant colonic tissues. *IEEE Trans Biomed Eng* **46** (10), 1246–1252.

[17] Fairman GS, Nathanson MH, West AB, Deckelbaum LI, Kelly L, and Kapadia CR (1995). Differences in laser-induced autofluorescence between adenomatous and hyperplastic polyps and normal colonic mucosa by confocal microscopy. *Dig Dis Sci* **40** (6), 1261–1268.

[18] Izuishi K, Tajiri H, Fujii T, Boku N, Ohtsu A, Ohnishi T, Ryi M, Kinoshita T, and Yoshida S (1999a). The histological basis of detection of adenoma and cancer in the colon by autofluorescence endoscopic imaging. *Endoscopy* **31** (7), 511–516.

[19] Bottiroli G, Croce AC, Locatelli D, Marchesini R, Pignoli E, Tomatis S, Cuzzoni C, Di Palma S, Dalfante M, and Spinellu P (1995). Natural fluorescence of normal and neoplastic human colon: a comprehensive "*ex vivo*" study. *Lasers Surg Med* **16** (1), 48–60.

[20] Zonios GI, Cothren RM, Arendt JT, Wu J, Van Dam J, Crawford JM, Manoharan R, and Feld MS (1996). Morphological model of human colon tissue fluorescence. *IEEE Trans Biomed Eng* **43** (2), 113–122.

[21] DaCosta RS, Ligle L, and Kost J, et al. (1997). Confocal microscopy/macroscopy and microspectrofluorimetry analysis of human colorectal tissue. *J Anal Morphol* **4**, 192–194.

[22] Glassman WS, Steinberg M, and Alfano RR (1994a). Time resolved and steady state fluorescence spectroscopy from normal and malignant cultured human breast cell lines. *Lasers Life Sci* **6** (2), 91–98.

[23] Anidjar M, Cussenot O, Blais J, Bourdon O, Avrillier S, Ettori D, Villter JM, Fiet J, Teillac P, and Le Duc A (1996a). Argon laser induced autofluorescence may distinguish between normal and tumor human urothelial cells: a microspectrofluorimetric study. *J Urol* **155** (5), 1771–1774.

[24] Ghadially FN, Neish WJP, and Dawkins HC (1963). Mechanisms involved in the production of red fluorescence of human and experimental tumors. *J Pathol Bacteriol* **85**, 77–92.

[25] Cheong WF, and Welch AJ (1990). A review of the optical properties of tissues. *IEEE J Quantum Electron* **26**, 2166–2185.

[26] Brown SB (1980). *An Introduction to Spectroscopy for Biochemists*. Academic Press, London, England.

[27] Koenig F, McGovern FJ, Enquist H, Larne R, Deutsch TF, and Schomacker KT (1998). Autofluorescence guided biopsy for the early diagnosis of bladder carcinoma. *J Urol* **159** (6), 1871–1875.

[28] Richards-Kortum R, Mehta A, Hayes G, Cothren RM, Kolubayev T, Kitrell C, Ratliff NB, Kramer JR, and Feld MS (1989). Spectral diagnosis of atherosclerosis using an optical fiber laser catheter. *Am Heart J* **118** (2), 381.

[29] Richards-Kortum R (1995). Fluorescence spectroscopy of turbid media. In *Optical-Thermal Response of Laser-Irradiated Tissue*. AJ Welch and MJC van Gemert (Eds.). Plenum Press, New York.

[30] Keijzer M, Richards-Kortum R, Jacques SL, and Feld MS (1989). Fluorescence spectroscopy of turbid media: autofluorescence of the human aorta. *Appl Opt* **28**, 4286–4292.

[31] Bottiroli G, Croce AC, Locatelli D, Nano R, Giombelli E, Messina A, and Benericetti E (1998). Brain tissue autofluorescence: an aid for intraoperative delineation of tumor resection margins. *Cancer Detect Prev* **22** (4), 330–339.

[32] Mycek MA, Schomacker KT, and Nishioka NS (1998). Colonic polyp differentiation using time-resolved autofluorescence spectroscopy. *Gastrointest Endosc* **48** (4), 390–394.

[33] Lam S, Kennedy T, Unger M, Miller YE, Gelmont D, Rusch V, Gipe B, Howard D, LeRiche J, Coldman A, and Gazdar A (1998). Localization

of bronchial intraepithelial neoplastic lesions by fluorescence bronchoscopy. *Chest* **113** (3), 696–702.

[34] Benson RC, Meyer RA, Zaruba ME, and McKhann GM (1979). Cellular autofluorescence — Is it due to flavins? *J Histochem Cytochem* **27**, 44.

[35] Pollack MA, Taylor A, Taylor J, and Williams RJ (1942). Vitamins in cancerous tissue I. Riboflavin. *Cancer Res* **2**, 739.

[36] Zhang JC, Savage HE, Sacks PG, Delohery T, Alfano RR, Katz A, and Schantz SP (1997). Innate cellular fluorescence reflects alteration in cellular proliferation. *Lasers Surg Med* **20** (3), 319–331.

[37] Sacks PG, Savage HE, Levine J, Kolli VR, Alfano RR, and Schantz SP (1996). Native cellular fluorescence identifies terminal squamous differentiation of normal oral epithelial cells in culture: a potential chemoprevention biomarker. *Cancer Lett* **104** (2), 171–181.

[38] Lohmann W, Mussmann J, Lohmann C, and Kunzel W (1989a). Native fluorescence of unstained cryo-sections of the cervix uteri compared with histological observations. *Naturwissenschaften* **76** (3), 125–127.

[39] Lohmann W, and Paul E (1989b). Native fluorescence of unstained cryo-sections of the skin with melanomas and nevi. *Naturwissenschaften* **76** (9), 424–426.

[40] Lohmann W, and Kunzel S (1990a). Fluorescence tomographical studies on breast tissue with cancer. *Naturwissenschaften* **77** (10), 476–478.

[41] Lohmann W, Hirzinger B, Braun J, Schwemmle K, Muhrer KH, and Schulz A (1990b). Fluorescence studies on lung tumors. *Z Naturforsch, Section C. J Biosci* **45** (9–10), 1063–1066.

[42] Fryen A, Glanz H, Lohmann W, Dreyer T, and Bohle RM (1997). Significance of autofluorescence for the optical demarcation of field cancerization in the upper aerodigestive tract. *Acta Otolaryngol* **117**, 316–319.

[43] Kubelka P (1954). New contributions to the optics of intensely light scattering materials: Part II. Non-homogeneous layers. *J Opt Soc Am* **344**, 330–335.

[44] Jacques SL (1995). Monte-Carlo methods. In *Optical-Thermal Response of Laser-Irradiated Tissue.* AJ Welch and MJC van Gemert (Eds.). Plenum Press, New York.

[45] Chance B, Schoener B, Oshino R, Itshak F, and Nakase Y (1979). Oxidation–reduction ratio studies of mitochondria in freeze-trapped samples. *J Biol Chem* **254** (11), 4764–4771.

[46] Zeng H, MacAulay C, McLean DI, and Palcic B (1995). Spectroscopic and microscopic characteristics of human skin autofluorescence emission. *Photochem Photobiol* **61** (6), 639–645.

[47] Zeng H, MacAulay C, McLean DI, and Palcic B (1997) Reconstruction of *in vivo* skin autofluorescence spectrum from microscopic properties by Monte Carlo simulations. *J Photochem Photobiol B: Biol* **38** (2–3), 234–240.

[48] Andrejevic S, Savary JF, Fontolliet C, Monnier P, and van den Bergh HE (1996). 7,12-Dimethylbenz(*A*)anthracene-induced early squamous-cell carcinoma in the golden Syrian hamster: evaluation of an animal model and comparison with early forms of human squamous-cell carcinoma in the upper aerodigestive tract. *Int J Exp Pathol* **77**, 7–14.

[49] Shklar G (1972). Experimental oral pathology in the Syrian hamster. *Prog Exp Tumor Res* **16**, 518–538.

[50] Morris AL, and Reiskin AB (1965). Hamster cheek pouch response to varying lengths of carcinogen exposure. *J Dent Res* **44**, 664–667.

[51] Balasubramaniam S, Elangovan V, and Govindaswamy S (1995). Fluorescence spectroscopic identification of 7,12-dimethylbenz[*a*]anthracene-induced hamster buccal pouch carcinogenesis. *Carcinogenesis* **16** (10), 2461–2465.

[52] Vengadesan N, Aruna P, and Ganesan S (1998). Characterization of native fluorescence from DBMA-treated hamster cheek pouch buccal mucosa for measuring tissue transformation. *Br J Cancer* **77** (3), 391–395.

[53] Chen CT, Chiang HK, Chow SN, Wang CY, Lee YS, and Chiang CP (1998). Autofluorescence in normal and malignant human oral tissues and in DMBA-induced hamster buccal pouch carcinogenesis. *J Oral Pathol Med* **27** (10), 470–474.

[54] Wang CY, Chen CT, Chiang CP, Young ST, Chow SN, and Chiang HK (1999). A probability-based multivariate statistical algorithm for autofluorescence spectroscopic identification of oral carcinogenesis. *Photochem Photobiol* **69** (4), 471–477.

[55] Dhingra JK, Zhang X, McMillan K, Kabani S, Manoharan R, Itzkan I, Feld MS, and Shapshay SM (1998). Diagnosis of head and neck precancerous lesions in an animal model using fluorescence spectroscopy. *Laryngoscope* **108** (4 Pt 1), 471–475.

[56] Van der Breggen EWJ, Rem AI, Christian MM, Yang CJ, Calhoun KH, Sterenborg HJCM, and Motamedi M (1997). Spectroscopic detection of oral and skin tissue transformation in a model for squamous cell carcinoma: autofluorescence versus aminolevulinic acid acid-induced fluorescence. *IEEE J Sel Top* **QE2**, 997–1007.

[57] Pathak I, Davis N, Hsiang YN, Quenville NF, and Palcic B (1995). Detection of squamous neoplasia by fluorescence imaging comparing porfimer sodium fluorescence to tissue autofluorescence n the hamster cheek pouch model. *Am J Surg* **170** (5), 423–426.

[58] Glasgold R, Glasgold M, Savage H, Pinto J, Alfano R, and Schantz S (1994). Tissue autofluorescence as an intermediate endpoint in NMBA-induced esophageal malignancies. *Cancer Lett* **82** (1), 33–41.

[59] Nauta JM, Speelman OC, van Leengoed HL, Nikkels PG, Roodenburg JL, Star WM, Witjes MJ, and Vermey A (1997). *In vivo* photodetection of chemically induced pre-malignant lesions and squamous cell carcinoma of the rat palatal mucosa. *J Photochem Photobiol B: Biol* **39** (2), 156.

[60] Sterenborg HJCM (1995). *In vivo* autofluorescence of an unpigmented melanoma in mice. Correlation of spectroscopic properties to microscopic structure. *Melanoma Res* **5**, 211–216.

[61] Stokes GG (1852). Uber die andung der brechbarkeit des lichtes. *Philos Trans R Soc* **107**, 11.

[62] Stubel H (1911). Die fluorezenz tierischer gewebe in ultravioletten licht. *Pflugers Arch Physiol* **142**, 1.

[63] Policard A (1924). Etudes sur les aspects offerts par des tumeurs experimentales examinees a la lumiere de Woods. *CR Soc Biol* **91**, 1423–1425.

[64] Lycette RM, and Leslie RB (1965). *Lancet* **2**, 436.

[65] Profio AE, and Doiron DR (1977). A feasibility study of the use of fluorescence bronchoscopy for the localization of small lung tumors. *Phys Med Biol* **22**, 949–957.

[66] Alfano RR, Tata DB, Cordero J, Tomashefsky P, Longo FW, and Alfano MA (1984). Laser induced fluorescence spectroscopy from native cancerous and normal tissue. *IEEE J Quantum Electron* **20**, 1507–1511.

[67] Lohmann W (1988). *in situ* detection of melanomas by fluorescence measurements. *Maturwissenschaften* **75**, 201–202.

[68] Yang Y, Ye Y, Li F, Li Y, and Ma P (1987). Characteristic autofluorescence for cancer diagnosis and its origin. *Lasers Surg Med* **7**, 528–532.

[69] Cothren RM, Sivak MV, Jr., Van Dam J, Petras RE, Fitzmaurice M, Crawford JM, Wu J, Brennan JF, Rava RP, Manoharan R, and Feld MS (1996). Detection of dysplasia at colonoscopy using laser induced fluorescence: a blinded study. *Gastrointest Endosc* **44** (2), 168–176.

[70] Ramanujam N, Mitchell MF, Mahadevan-Jansen A, Thomsen S, Staerkel G, Malpica A, Wright T, Atkinson A, and Richards-Kortum R (1996c). Cervical pre-cancer detection using a multivariate statistical algorithm based on laser induced fluorescence spectra at multiple excitation wavelengths. *Photochem Photobiol* **64**, 720–735.

[71] Tumer K, Ramanujam N, Ghosh J, and Richards-Kortum R (1998). Ensembles of radial basis function networks for spectroscopic detection of cervical precancer. *IEEE Trans Biomed Eng* **45** (8), 953–961.

[72] Brookner CK, Utzinger U, Staerkel G, Richards-Kortum R, and Mitchell MF (1999). Cervical fluorescence of normal women. *Lasers Surg Med* **24**, 29–37.

[73] Kulapaditharom B, and Boonkitticharoan V (1998a). Laser induced fluorescence imaging in localization of head and neck cancers. *Ann Otol, Rhinol, Laryngol* **107** (3), 241–246.

[74] Kulapaditharom B, Boonkitticharoan V, and Kunachak (1998b). Fluorescence guided biopsy in the diagnosis of an unknown primary cancer in patients with metastatic cervical lymph nodes. *Ann Otol, Rhinol, Laryngol* **108**, 700–704.

[75] Zargi M, Smid L, Fajdiga I, Bubnic B, Lenarcic J, and Oblak P (1997a). Laser induced fluorescence in diagnostics of laryngeal cancer. *Acta Oto-Laryngol, Suppl* **527**, 125–127.

[76] Zargi M, Smid L, Fajdiga I, Bubnic B, Lenarcic J, and Oblak P (1997b). Detection and localization of early laryngeal cancer with laser induced fluorescence: a preliminary report. *Eur Arch Oto-Rhino-Laryngol, Suppl* **2**, S113–S116.

[77] Izuishi K, Tajiri H, Ryu M, Furuse J, Maru Y, Inoue K, Konishi M, and Kinoshita T (1999b). Detection of bile duct cancer by autofluores-

cence cholangioscopy: a pilot study. *Hepato-Gastroenterology* **46** (26), 707–804.

[78] Richards-Kortum R, Rava RP, Petras RE, Fitzmaurice M, Sivak M, and Feld MS (1991). Spectroscopic diagnosis of colonic dysplasia. *Photochem Photobiol* **53** (6), 777–786.

[79] Kapadia CR, Cutruzzola FW, O'Brien KM, Stetz ML, Enriquez R, and Deckelbaum LI (1990). Laser-induced fluorescence spectroscopy of human colonic mucosa. Detection of adenomatous transformation. *Gastroenterology* **99** (1), 150–157.

[80] Yang Y, Tang GC, Bessler M, and Alfano RR (1995). Fluorescence spectroscopy as a photonic pathology method for detecting colon cancer. *Lasers Life Sci* **6** (4), 259–276.

[81] Chwirot BW, Michniewicz Z, Kowalska M, and Nussbeutel J (1998a). Detection of colonic malignant lesions by digital imaging of UV laser-induced autofluorescence. *Photochem Photobiol* **69** (3), 336–340.

[82] Wang TD, Van Dam J, Crawford JM, Presinger EA, Wang Y, and Feld MS (1996). Fluorescence endoscopic imaging of human colonic adenomas. *Gastroenterology* **111**, 1182–1191.

[83] Schomacker KT, Frisoli JK, Compton CC, Flotte TJ, Richter JM, Deutsch TF, and Nishioka NS (1992a). Ultraviolet laser-induced fluorescence of colonic polyps. *Gastroenterology* **102** (4 Pt 1), 1155–1160.

[84] Schomacker KT, Frisoli JK, Compton CC, Flotte TJ, Richter JM, Nishioka NS, and Deutsch TF (1992b). Ultraviolet laser-induced fluorescence of colonic tissue: basic biology and diagnostic potential. *Lasers Surg Med* **12** (1), 63–78.

[85] Eker C, Montan S, Jaramillo E, Koizumi K, Rubio C, Andersson-Engels S, Svanberg K, Svanberg S, and Slezak P (1999). Clinical spectral characterization of colonic mucosal lesions using autofluorescence and delta amniolevulinic acid sensitization. *Gut* **44** (4), 511–518.

[86] Cothren RM, Richards-Kortum R, Sivak MV, Jr., Fitzmaurice M, Rava RP, Boyce GA, Doxtader M, Blackman R, Ivanc TB, and Hayes GB, et al. (1990). Gastrointestinal tissue diagnosis by laser-induced fluorescence spectroscopy at endoscopy. *Gastrointest Endosc* **36** (2), 105–111.

[87] Catalano MF, Van Dam J, Bedford R, Cothren RM, and Sivak MV, Jr. (1993). Preliminary evaluation of the prototype stereoscopic endoscope: precise three-dimensional measurement system. *Gastrointest Endosc* **39** (1), 23–28.

[88] Wang TD, Crawford JM, Feld MS, Wang Y, Itzkan I, and Van Dam J (1999). *In vivo* identification of colonic dysplasia using fluorescence endoscopic imaging. *Gastrointest Endosc* **49** (4 Pt 1), 447–455.

[89] Duvall GA, Kost J, and Cheider D, et al. (1996). Laser induced fluorescence endoscopy (LIFE): a pilot study of a real time autofluorescence imaging system for early detection of dysplasia and carcinoma in the GI tract. *Endoscopy* **28**, S45.

[90] DuVall GA, Wilson BC, and Marcon N (1997). Tissue autofluorescence. *Ann Gastrointest Endosc* **10**, 25–30.

[91] Lohmann W, Mussman J, Lohmann C, and Kunzel W (1989c). Native fluorescence of the cervix uteri as a marker for dysplasia and invasive carcinoma. *Eur J Obstet Gynecol Reprod Biol* **31**, 249–253.

[92] Glassman WS, Liu CH, Tang GC, Lubicz S, and Alfano RR (1992). Ultraviolet excited fluorescence spectra from non–malignant and malignant tissues of the gynecological tract. *Lasers Life Sci* **5**, 49–58.

[93] Glassman WS, Liu CH, Lubicz S, and Alfano RR (1994b). Excitation spectroscopy of malignant and nonmalignant gynecological tissues. *Lasers Life Sci* **6**, 99–106.

[94] Mahadevan A, Mitchell MF, Silva E, Thomsen S, and Richards-Kortum R (1993). Study of the fluorescence properties of normal and neoplastic human cervical tissue. *Lasers Surg Med* **13** (6), 647–655.

[95] Ramanujam N, Mitchell MF, Mahadevan A, Thomsen S, Silva E, and Richards-Kortum R (1994a). Fluorescence spectroscopy: a diagnostic tool for cervical intraepithelial neoplasia (CIN). *Gynecol Oncol* **52**, 31–38.

[96] Ramanujam N, Mitchell MF, Mahadevan A, Thomsen S, and Richards-Kortum R (1994b). *In vivo* diagnosis of cervical intraepithelial neoplasia (CIN) using 337 nm laser induced fluorescence. *Proc Natl Acad Sci* **91**, 10193–10197.

[97] Ramanujam N, Mitchell MF, Mahadevan A, Thomsen S, Malpica A, Wright T, Atkinson A, and Richards-Kortum R (1996a). Development of a multivariate statistical algorithm to analyze human cervical tissue fluorescence spectra acquired *in vivo*. *Lasers Surg Med* **19** (1), 46–62.

[98] Ramanujam N, Mitchell MF, Mahadevan A, Thomsen S, Malpica A, Wright T, Atkinson A, and Richards-Kortum R (1996b). Spectroscopic diagnosis of cervical intraepithelial neoplasia (CIN) *in vivo* using laser-induced fluorescence spectra at multiple excitation wavelengths. *Lasers Surg Med* **19** (1), 63–72.

[99] Brookner CK, Agrawal A, Trujillo EV, Mitchell MF, and Richards-Kortum R (1997). Safety analysis: relative risks of ultraviolet exposure from fluorescence spectroscopy and colposcopy are comparable. *Photochem Photobiol* **65** (6), 1020–1025.

[100] Agrawal A, Utzinger U, Brookner C, Pitris P, Mitchell MF, and Richards-Kortum R (1999). Fluorescence spectroscopy of the cervix: influence of acetic acid, cervical mucus and vaginal medications. *Lasers Surg Med* **25**, 237–249.

[101] Mitchell MF, Cantor SB, Ramanujam N, Tortolero-Luna G, and Richards-Kortum R (1999). Fluorescence spectroscopy for the diagnosis of squamous intraepithelial lesions of the cervix. *Obstet Gynecol* **93** (3), 462–470.

[102] Cantor SB, Mitchell MF, Tortolero-Luna G, Bratka CS, Bodurka DC, and Richards-Kortum R (1999). Cost-effectiveness analysis of diagnosis and management of cervical squamous intraepithelial lesions. *Obstet Gynecol* **91** (2), 270–277.

[103] Koumantakis E, Vasileiou A, Makrigiannakis A, Unsold E, and Papazoglou TG (1997). Spectral variations of laser induced tissue emission during *in vivo* detection of malignancies in the female genital tract. *J Photochem Photobiol* **B40**, 183–186.

[104] Hung J, Lam S, LeRiche J, and Palcic B (1991). Autofluorescence of normal and malignant bronchial tissue. *Lasers Surg Med* **11**, 99–105.

[105] Palcic B, Lam S, and Hung J, et al. (1991). Detection and localization of early lung cancer by imaging techniques. *Chest* **99**, 742–743.

[106] Lam S, Hung J, and Palcic B (1991). Mechanism of detection of early lung cancer by ratio fluorimetry. *Lasers Life Sci* **4**, 67–73.

[107] Lam S, Hun JY, Kennedy SM, LeRiche JC, Vedal S, and Nelams B, et al. (1992). Detection of dysplasia and carcinoma *in situ* by ratio fluorimetry. *Am Rev Respir Dis* **146**, 1458–1461.

[108] Lam S, MacAulay C, Hung J, LeRiche J, Profio AE, and Palcic B (1993a). Detection of dysplasia and carcinoma *in situ* with a lung imaging fluorescence bronchoscope device. *J Thorac Cardiovasc Surg* **105**, 1035–1040.

[109] Lam S, MacAulay C, and Palcic B (1993b). Detection and localization of early lung cancer by imaging techniques. *Chest* **103**, 12S–14S.

[110] Lam S, MacAulay C, and LeRiche J, et al. (1994). Early localization of bronchogenic carcinoma. *Diagn Ther Endosc* **1**, 75–78.

[111] Harries ML, Lam S, MacAulay C, Qu JA, and Palcic B (1995). Diagnostic imaging of the larynx: autofluorescence of laryngeal tumors using the helium cadmium laser. *J Laryngol Otol* **109**, 108–110.

[112] D'Hallewin MA, Baert L, and Vanherzeele H (1994). Fluorescence imaging in bladder cancer. *Acta Urol Belg* **62**, 49.

[113] Baert L, Berg R, Van Damme B, D'Hallewin MA, Johansson J, Svanberg K, and Svandberg S (1993). Clinical fluorescence diagnosis of human bladder carcinoma following low dose photofrin injection. *Urol* **41**, 322.

[114] Koenig F, McGovern FJ, Althausen AF, Deutsch TF, and Schomacker KT (1996). Laser induced autofluorescence diagnosis of bladder cancer. *J Urol* **156** (5), 1597–1601.

[115] Anidjar M, Ettori D, Cussenot O, Meria P, Desgrandchamps F, Cortesse A, Teillac P, Le Duc A, and Avrillier S (1996b). Laser induced autofluorescence of bladder tumors: dependence on excitation wavelength. *J Urol* **156** (5), 1590–1596.

[116] Montan S, and Strombland LG (1987). Spectral characterization of brain tumors utilizing laser-induced fluorescence. *Lasers Life Sci* **1**, 275–285.

[117] Panjehpour M, Overholt BF, Schmidhammer JL, Farris C, Buckley PF, and Vo-Dinh T (1995). Spectroscopic diagnosis of esophageal cancer: new classification model, improved measurement system. *Gastrointest Endosc* **41**, 577–581.

[118] Vo-Dinh T, Panjehpour M, Overholt BF, Farris C, Buckley FP III, and Sneed R (1995). *In vivo* cancer diagnosis of the esophagus using differentialized normalized fluorescence (DNF) indices. *Laser Surg Med* **16**, 41–47.

[119] Panjehpour M, Overholt BF, Vo-Dinh T, Haggit RC, Edwards DH, and Buckely FP III (1996). Endoscopic fluorescence detection of high grade dysplasia in Barrett's esophagus. *Gastroenterology* **111**, 93–101.

[120] Ingrams DR, Dhingra JK, Roy K, Perrault DF, Jr., Bottrill ID, Kabani S, Rebeiz EE, Pankratov MM, Shapshay SM, Manoharan R, Itzkhan I, and Feld MS (1997). Autofluorescence characteristics of oral mucosa. *Head Neck* **19** (1), 27–32.

[121] Majumder SK, Gupta PK, and Uppal A (1999). Autofluorescence spectroscopy of tissues from human oral cavity for discriminating malignant from normal. *Lasers Life Sci* **8** (4), 211–227.

[122] Yang CY, Chiang HK, Chen CT, Chaing CP, Kuo YS, and Chow SN (1999). Diagnosis of oral cancer by light-induced autofluorescence spectroscopy using double excitation wavelengths. *Oral Oncol* **35**, 144–150.

[123] Kolli VR, Savage HE, and Schantz SP (1995). Native cellular fluorescence of neoplastic aerodigestive tract mucosa. *Arch Otolaryngol, Head Neck Surg* **121**, 1287–1292.

[124] Dhingra JK, Perrault DF, McMillan K, Rebeiz EE, Kabani S, Manoharan R, Itzkan I, Feld MS, and Shapshay SM (1996). Early diagnosis of upper aerodigestive tract cancer by autofluorescence. *Arch Otolaryngol, Head Neck Surg* **122** (11), 1181–1186.

[125] Gillenwater A, Jacob R, Ganeshappa R, Kemp B, El-Naggar AK, Palmer JL, Clayman G, Mitchell MF, and Richards-Kortum R (1998a). Noninvasive diagnosis of oral neoplasia based on fluorescence spectroscopy and native tissue autofluorescence. *Arch Otolaryngol, Head Neck Surg* **124** (11), 1251–1258.

[126] Gillenwater A, Jacob R, and Richards-Kortum R (1998b). Fluorescence spectroscopy: a technique with potential to improve the early detection of aerodigestive tract neoplasia. *Head Neck* **20** (6), 556–562.

[127] Betz CS, Mehlmann M, Rick K, Stepp H, Grevers G, Baumgartner R, and Leunig A (1999). Autofluorescence imaging and spectroscopy of normal and malignant mucosa in patients with head and neck cancer. *Lasers Surg Med* **25**, 323–334.

[128] Lohmann W, Nilles M, and Boedeker RH (1991). *In situ* differentiation between nevi and malignant melanomas by fluorescence measurements. *Naturwissenschaften* **78**, 456–457.

[129] Sterenborg HJCM, Motamedi M, Wagner RF, Duvic M, Thomsen S, and Jacques SL (1994). *In vivo* fluorescence spectroscopy and imaging of human skin tumors. *Lasers Med Sci* **9**, 191–201.

[130] Chwirot BW, Chwirot S, Redzinski J, and Michiniewicz Z (1998b). Detection of melanomas by digital imaging of spectrally resolved ultraviolet light induced autofluorescence of human. *Eur J Cancer* **34** (11), 1730–1734.

[131] Alfano RR, Tang GC, Pradhan A, Lam W, Choy DSJ, and Opher E (1987). Fluorescence spectra from cancerous and normal breast and lung tissue. *IEEE J Quantum Electron* **23**, 1806–1811.

[132] Yang Y, Katz A, Celmer EJ, Zurawska-Szczepaniak M, and Alfano RR (1996). Optical spectroscopy of benign and malignant tissues. *Lasers Life Sci* **7** (2), 115–127.

[133] Yang Y, Katz A, Celmer EJ, Zurawska-Szczepaniak M, and Alfano RR (1997). Excitation spectrum of malignant and benign breast tissues: a potential optical biopsy approach. *Lasers Life Sci* **7** (4), 249–265.

[134] Gupta PK, Majumder SK, and Uppal A (1997). Breast cancer diagnosis using nitrogen laser excited autofluorescence spectroscopy. *Lasers Surg Med* **21** (5), 417–422.

[135] Chwirot BW, Chwirot S, Jedrzejczyk W, Jackowski M, Raczynska AM, Winczakiewicz J, and Dobber J (1997). Ultraviolet laser induced fluorescence of human stomach tissues: detection of cancer tissues by imaging techniques. *Lasers Surg Med* **21** (2), 149–158.

[136] Zangaro RA, Silveira L, Jr., Manoharan R, Zonios G, Itzkan I, Dasari RR, Van Dam J, and Feld MS (1996). Rapid multiexcitation fluorescence spectroscopy system for *in vivo* tissue diagnosis. *Appl Opt* **35** (25), 5211–5219.

[137] Zuluaga AF, Utzinger U, Durkin AJ, Holger F, Gillenwater A, Jacob R, Kemp B, Fan J, and Richards-Kortum R (1999). Fluorescence excitation and emission matrices of human tissues: a system for *in vivo* measurement and method of data analysis. *Appl Spectrosc* **53** (3), 302–311.